

THE MELILITE-BEARING HIGH-TEMPERATURE SKARNS OF THE APUSENI MOUNTAINS, CARPATHIANS, ROMANIA

MARIE-LOLA PASCAL[§]

CNRS-ISTO (Institut des Sciences de la Terre d'Orléans), 1A, rue de la Férollerie, F-45071 Orléans Cedex 02, France

MICHEL FONTEILLES

Laboratoire de Pétrologie, Université Pierre-et-Marie-Curie, 4, place Jussieu, F-75252 Paris Cedex 05, France

JEAN VERKAEREN AND RÉGIS PIRET

*Unité de Géologie, Université Catholique de Louvain-la-Neuve, Batiment Mercator, 3, place Louis Pasteur,
B-1348 Louvain-la-Neuve, Belgium*

ȘTEFAN MARINCEA

Geological Institute of Romania, 1, Caransebes Street, RO-78344 Bucharest, Romania

ABSTRACT

The melilite-bearing skarns of Cornet Hill (CH) and Upper Cerboia Valley (UCV), in the Apuseni Mountains of Romania, occur at the contact between monzodiorite bodies of Ypresian age (Paleocene) and Neojurassic calcitic marbles. Typical wollastonite – grossular – diopside endoskarns are separated from exoskarns (tilleyite and spurrite or wollastonite at CH, wollastonite only at UCV), at most places, by a melilite-rich rock, in which veins and vein-like zones of recrystallization are composed only of idiomorphic melilite crystals reaching 15 cm across. Titanian garnet and wollastonite are the principal minerals associated with melilite (and also monticellite, perovskite, vesuvianite, cuspidine, spurrite, tilleyite, calcite, hydroxyllellastadite, hydrogrossular and other minor alteration-induced minerals). A different association that includes aluminian diopside and grossular occurs (1) as veinlets in the marble close to the skarns and (2) as relict inclusions in endoskarns. From the geometrical relationships of the zone sequences and the veins, the textural features of the mineral associations and the inferred conditions of fluid–mineral equilibrium, these mineralogical peculiarities are interpreted as resulting from the superposition of two main stages. Firstly, there was circulation of a comparatively CO₂-rich fluid formed the early aluminian diopside – grossular endoskarns, with depletion in Si (and Fe, Na, K) and inert behavior of Mg, Al, Ti. Then, a high-temperature (750°C) fluid circulated on both sides of the contact between marble and endoskarns, and developed the melilite-rich, titanian-garnet-bearing rocks partly at the expense of previously formed endoskarns, and spurrite or wollastonite (CH) or wollastonite (UCV) exoskarns at the expense of marble. The pressure of CO₂ was very low, less than 26 bars at UCV and 16 bars at CH, with a H₂O pressure less than 750 bars. Not only Si and Ca were mobilized, but also Mg, Al and Ti, leached from the endoskarns and deposited in the veins and the nearby part of exoskarns. This stage, which occurred in the temperature range corresponding to the end of the crystallization of plagioclase in the monzodiorite, has pegmatitic chemical and textural features. The main flow of fluid ended with the development of tilleyite partly at the expense of spurrite and wollastonite at CH, and local high-temperature (about 710°C) recrystallization of the zonation, mostly in veins, especially in the endoskarn–exoskarn boundary, but also within the endoskarns. A monticellite – gehlenite association appeared in the melilite-rich rocks, later followed by vesuvianite, whereas in the endoskarn, vesuvianite developed together with coarse-grained wollastonite and grossular.

Keywords: skarns, melilite, spurrite, tilleyite, titanian garnet, metasomatism, Apuseni Mountains, Romania.

SOMMAIRE

Les skarns à mélilite de Cornet Hill (CH) et de la haute vallée de la Cerboia (UCV), dans les monts Apuseni, en Roumanie, sont développés au contact de corps intrusifs monzodioritiques, d'âge Ypresien (Paléocène), aux dépens de ceux-ci et des marbres encaissants, purement calcitiques, d'âge néojurassique. Les endoskarns typiques, caractérisés par l'association wollastonite – grossulaire – diopside, sont séparés des exoskarns (wollastonite à UCV, tilleyite et spurrite ou wollastonite à CH) par une roche

[§] E-mail address: mlpascal@cnrs-orleans.fr

à méililite dominante, d'épaisseur variable, localement absente, comportant des veines et des recristallisations uniquement formées de méililite en cristaux idiomorphes atteignant 15 cm. Les principaux minéraux associés à la méililite sont le grenat titanifère et la wollastonite, auxquels s'ajoutent monticellite, pérovskite, vésuvianite, cuspidine, spurrite, tilleyite, calcite, hydroxyllestadite, hydrogrossulaire et divers minéraux d'altération. Une paragenèse différente, comportant diopside alumineux et grossulaire, apparaît soit en veinules dans le marbre à proximité immédiate des skarns, soit en reliques dans l'endoskarn. À partir des relations géométriques entre séquences de zones et veines, des compositions des minéraux et de leurs relations texturales, et de la modélisation thermochimique de leurs conditions de stabilité, ces particularités sont interprétées par la superposition de deux processus hydrothermaux de haute température et basse pression [750°C, P(H₂O) < 750 bars], chimiquement contrastés: 1) formation d'endoskarn précoces à diopside alumineux – grossulaire, par un fluide relativement riche en CO₂ [P(CO₂) > 100 bars] qui lessive Si, Fe, Na, K sans mobiliser Mg, Al et Ti. 2) Circulation, le long du contact entre marbres et endoskarns, d'un fluide caractérisé par une très faible pression de CO₂ (moins de 26 bars à UCV, moins de 16 bars à CH), qui développe la méililite et le grenat titanifère en veines et aux dépens des endoskarns, et transforme le marbre en spurrite ou wollastonite à CH, en wollastonite à UCV. Les transformations observées impliquent un apport de Mg, Al, Si et Ti dans les exoskarns proches du contact, et un lessivage de Mg et Ti dans les endoskarns. Par ses particularités chimiques et texturales et en accord avec sa température, qui correspond à la fin de cristallisation de la monzodiorite, ce processus présente un caractère pegmatitique. Ce stade évolue avec le développement de la tilleyite à CH, en partie aux dépens de la spurrite et de la wollastonite, et prend fin vers 710°C avec des modifications secondaires locales, principalement en veines: dans les roches à méililite apparaissent une association à monticellite – gehlenite, puis la vésuvianite, et dans l'endoskarn, la vésuvianite et des recristallisations de la wollastonite et du grenat.

Mots-clés: skarns, méililite, spurrite, tilleyite, grenat titanifère, métasomatose, monts Apuseni, Roumanie.

INTRODUCTION

The skarn occurrences to be described here are located in the Apuseni Mountains of Romania, about 20 km west of the town of Brad. Istrate *et al.* (1978), Stefan *et al.* (1978) and Piret (1997) have reported the presence of high-temperature minerals such as melilite, spurrite and tilleyite in these skarns. Few occurrences of such minerals have been described in literature. Some are products of high-grade metamorphism of siliceous limestone [e.g., Carlingford, Ireland: Nockolds (1947), Camas Mor, Scotland: Tilley (1948, 1951), Tunguska River basin, Siberia: Reverdatto (1970), Reverdatto *et al.* (1979), and Hatrurim, Israel: Gross (1977)], or of calcic enclaves in melts [Oslo Rift: Jamtveit *et al.* (1992, 1997), Willemse & Bensch (1964)]. Others are skarn associations [e.g., Crestmore, California: Burnham (1959), Wiechmann (1995), Scawt Hill, Ireland: Tilley (1929), Carneal, Ireland: Sabine (1975), Isle of Rhum, Scotland: Hughes (1960), Christmas Mountains, Texas: Joesten (1974), Joesten & Fisher (1988), Kushiro, Japan (Henmi *et al.* 1971), and Fuka, Japan (Henmi *et al.* 1973)]. Of these, the Crestmore occurrence has been the focus of particular attention by mineralogists and petrologists and constitutes a reference for this peculiar type of skarn.

The classical interpretation of skarn formation involves (i) the infiltration of a magmatic fluid into the surrounding rocks and (ii) the development of a sequence of continuous zones tending to be monomineralic, according to the chromatographic model (Korzhinskii 1970). Where skarn veins are observed, they should represent the most thoroughly fluid-controlled part of the system, and the zone sequences are expected to be organized around them. However, in the skarns at Crestmore, the associations described by Burnham (1959) in the monticellite zone show neither a

continuous development nor a tendency to a monomineralic character. These skarns thus cannot be completely described as a chromatographic sequence. The existence in skarns of hydrothermal processes other than the outward infiltration of a magmatic fluid is also indicated by available isotopic signatures (O, H) of skarn minerals, which commonly indicate a dominantly metamorphic origin for the fluid (Guy *et al.* 1988). In addition, a large-scale development of typical endoskarns is easier to account for in the case of a (locally) external origin for part of the fluids.

The high temperature that characterizes the mineral associations of the skarns of the Apuseni Mountains indicates that products of the early metasomatic processes have not been extensively reworked by late hydrothermal circulation; therefore, these skarns are appropriate to illustrate those features than can be attributed to the chromatographic model from those that cannot. As the veins and their geometrical and chronological relations to the zonal pattern offer clues relevant to this issue, they have been described with the same detail as the zonal sequences, in order to decide which minerals, with which compositions, were associated at equilibrium.

GEOLOGICAL SETTING AND FIELD RELATIONSHIPS

In the region of Magureaua Vatei (Fig. 1), the geological formations include a thick (>3000 m) sequence of calc-alkaline mafic volcanic rocks and gabbros, the "ophiolites" of Drocea, of Upper Triassic to Jurassic age. Neojurassic limestones follow, overlain by Cretaceous clastic sediments and Upper Mesozoic basalts and andesites. This sequence is cut by felsic hypabyssal bodies of Ypresian age (Paleocene), the so-called banatites, ranging in composition from dominant monzodiorite to minor monzonite, syenite and granite

(mainly granite porphyry and granophyre), at the contact of which the high-temperature skarns have been observed. Two occurrences are described here: (1) a very small one on top of Cornet Hill (CH), where the contact outcrops over twenty meters, and (2) an even smaller outcrop of an intrusive contact in the Upper Cerboia Valley (UCV).

In both occurrences, the host marble is exclusively composed of pure calcite. At any one place, the original contact is masked by several sequences of mineral associations, of which 52 samples were collected. The sequences mainly differ by the mineralogical nature of the exoskarms, spurrite – tilleyite \pm wollastonite at CH, wollastonite \pm calcite at UCV. Two sequences are described below; sequence S is from Cornet Hill, and sequence W is from the Upper Cerboia Valley.

Sequence S

Over a few meters at the contact with the quartz monzodiorite, Istrate *et al.* (1978) reported the following zonation: quartz monzodiorite / wollastonite + melilite + vesuvianite / spurrite / tilleyite / calcite. According to our observations, the wollastonite – melilite – vesuvianite zone of Istrate *et al.* (1978) includes two distinct parts. One is composed of wollastonite – grossular \pm pyroxene (zone A, Table 1), and the other, of melilite as the dominant mineral (zone B). The spurrite and tilleyite zones of Istrate *et al.* (1978) (C and D), mainly composed of very coarse-grained carbonate-bearing minerals (with some wollastonite, melilite, titanian garnet, and vesuvianite), are interpreted as exoskarms. According to the field observations of Istrate *et al.* (1978), the zones are reported to be several meters wide, but as they occur as a back-slope, with rather poor conditions of outcrop, the thicknesses may have been overestimated; no transverse section exists through this system of zones.

The succession of mineral associations shown in Table 1 is that obtained after eliminating secondary modifications and alterations, which are examined in detail in a companion paper by Marincea *et al.* (2001). The specific minerals are listed with their structural formulae in Table 2. As spurrite, of major petrological significance, has been observed only in a few samples, Table 1 shows the spurrite-free sequence as the main one, and the location of spurrite-bearing zones as variants of the sequence. Most skarn samples can be located in this sequence of zones. One sample (CH22) shows a wollastonite exoskarn zone without melilite, the exoskarn being in direct contact with typical grossular – wollastonite endoskarms (zone A).

Sequence W

The only difference between sequence W and sequence S is the absence of spurrite and tilleyite. The exoskarn (zone C), composed of calcite – wollastonite

(with some melilite and titanian garnet), is in contact with zone B, containing the assemblage melilite – wollastonite – titanian garnet.

Melilite veins

The boundary between zones B and C is occupied by a vein (“BV”) a few mm thick at CH and up to 1 m at UCV, composed of coarse melilite (up to 0.5 cm at CH, more than 15 cm at UCV) (Plates 1B and 2 in Stefan *et al.* 1978). Many similar veinlets of melilite (in most cases associated with titanian garnet), millimeters in thickness at CH and centimeters at UCV, have been observed in exoskarms, branching off the main vein (Fig. 2).

Pyroxene veins

In the marble at UCV, very close to the melilite – wollastonite rock and one meter away from the quartz monzonite, a complicated and dense network of veinlets, at most a few mm thick, is mainly composed of pyroxene and garnet (sample UCV4–1).

PETROGRAPHY OF THE INTRUSIVE ROCKS

Monzodiorites

The primary minerals present in the monzodiorite includes abundant plagioclase (An_{40–60}, An₂₅ at the rim), some orthopyroxene or amphibole (or both), much clinopyroxene and biotite, magnetite and ilmenite, K-feldspar and quartz. Accessory minerals are apatite and scarce zircon. The most important difference between CH and UCV localities is the occurrence at CH of small early phenocrysts of greyish Ti-bearing edenite, whereas at UCV a brownish Ti-rich edenite is only observed as inclusions in the center of zoned grains of clinopyroxene.

K-feldspar shows a tendency to concentrate in patches (monzonitic texture). In many samples, at least part of the quartz appears to be late to develop, mainly at the expense of K-feldspar. Interstitial granophyre is still locally observed, and may constitute up to 80% of the rock, as in sample UCV3, in which the other constituents are the same as in the normal monzodiorite (*e.g.*, same composition of orthopyroxene). The amounts of K-feldspar and quartz are highly variable, even at the scale of the hand specimen (UCV63), suggesting an appreciable mobility of the pegmatite-forming melt with respect to the already crystallized dioritic framework of the rock. This melt, either granitic or syenitic, shows a tendency to concentrate in the margins of the intrusive body.

Contaminated rocks and “syenite”

Close to the contact with the skarns, some changes in the associations of the intrusive rocks, especially in

TABLE 1. SIMPLIFIED MINERALOGICAL COMPOSITION OF THE SKARN ZONES IN SEQUENCE S, CORNET HILL, ROMANIA

Zone D	Zone C	Veins (BV) at B - C	Zone B	Zone A3	Zone A2	Zone A1	"Syenite"
Tly	Wo	<i>Spr</i> *	Wo	Wo	Wo	Wo	
Cal	<i>Spr</i> *	Mel	Mel	Grs	Grs	Grs	Kfs
	Tly	<i>Prv</i> *	tit. Grt	tit. Grt	Di	Cpx [‡]	Cpx [‡]
	Cal	tit. Grt				Prv	Ttn

* Observed as a local variant of the sequence. † Na-bearing Cpx, ‡ Na-rich Cpx. Symbols: Cal calcite, Cpx clinopyroxene, Di diopside, Grs grossular, tit. Grt titaniferous garnet, Mel Mellilite, Prv perovskite, Spr spurrite, Tly tilleyite, Ttn titanite, Wo wollastonite.

TABLE 2. SPECIFIC MINERALS REFERRED TO IN THE DESCRIPTION OF SKARNS FROM CORNET HILL AND UPPER CERBOAIA VALLEY, ROMANIA

Name	Structural formula
Åkermanite	$\text{Ca}_2\text{MgSi}_2\text{O}_7$
Aluminian diopside	$\text{CaMg}_{1-x}(\text{Al,Fe}^{3+})_2\text{Si}_{2-x}\text{O}_6$
Bicchulite	$\text{Ca}_2\text{Al}_2\text{SiO}_4(\text{OH})_2$
CaTs clinopyroxene	$\text{CaAl}_2\text{SiO}_6$
Cebollite	$\text{Ca}_2(\text{Mg,Fe}^{2+},\text{Al})\text{Si}_2(\text{O,OH})_4$
Cuspidine	$\text{Ca}_{16}(\text{Si}_2\text{O}_7)_4(\text{F,OH})_8$
Djerfisherite	$\text{K}_4(\text{Cu,Fe,Ni})_{23}\text{S}_{26}\text{Cl}$
Esseneite	$\text{CaFe}^{3+}\text{AlSiO}_6$
Gehlenite	$\text{Ca}_2\text{Al}_2\text{SiO}_7$
Foshagite	$\text{Ca}_2\text{Si}_2\text{O}_7(\text{OH})_2$
Hibschite	$\text{Ca}_2\text{Al}_2(\text{SiO}_3)_2(\text{OH})_{16}$
Hydroxyllellestadite	$\text{Ca}_4[(\text{SiO}_3)_2(\text{SO}_4)(\text{PO}_4)]_2(\text{OH,F,Cl})$
Kamaishiite	$\text{Ca}_2\text{Al}_2\text{SiO}_4(\text{OH})_2$
Mellilite	$(\text{Ca,Na})_2(\text{Al,Mg})(\text{Si,Al})_2\text{O}_7$
Monticellite	CaMgSiO_4
Mountainite	$\text{Ca}_2\text{Si}_2\text{O}_7 \cdot 3\text{H}_2\text{O}$
Perovskite	CaTiO_3
Rankinite	$\text{Ca}_2\text{Si}_2\text{O}_7$
Spurrite	$\text{Ca}_2(\text{SiO}_3)_2(\text{CO}_3)$
Tilleyite	$\text{Ca}_2\text{Si}_2\text{O}_7(\text{CO}_3)_2$
Titanian garnet	$\text{Ca}_3(\text{Fe}^{3+},\text{Al,Ti})_2(\text{Si,Al,Fe}^{3+})_3\text{O}_{12}$
Vesuvianite	$\text{Ca}_{10}\text{Mg}_2\text{Al}_4(\text{SiO}_3)_4(\text{Si}_2\text{O}_7)_2(\text{OH,F,O,Cl})$
Xonotlite	$\text{Ca}_2\text{Si}_2\text{O}_7(\text{OH})_2$

their pegmatitic parts, correspond to what is commonly attributed to contamination. At the contact with the endoskarms, the rock is referred to as "syenite". These changes show a more or less clearly defined zonal pattern, with at first the disappearance of ilmenite and the appearance of titanite. The corrosion of plagioclase is accompanied by the development of an association of K-feldspar, quartz and greenish clinopyroxene. Fine-grained polycrystalline aggregates of clinopyroxene, biotite and magnetite are pseudomorphic after orthopyroxene and hornblende, which completely disappear.

The next step is the disappearance of primary biotite, accompanied by the further development of clinopyroxene and, in syenitic varieties, by the formation of nepheline, interpreted as due to this silica-consuming reaction. Sample CH2, composed of large crystals of

nonperthitic and fresh alkali feldspar (Or_{64-68}) that include a multitude of unoriented very small idiomorphic crystals of oligoclase (An_{22-26}) and diopside (Di_{80}), is considered to represent the last stage of plagioclase stability, before a transition to typical alkali feldspar pegmatites, which occur as large veins in this rock. Such pegmatites include quartz-bearing and nepheline-bearing varieties. In some of them, the coarse-grained orthoclase (12–20% Ab, 0.20–0.37% An and 0.09–0.12 wt.% FeO) leaves large intercrystalline spaces filled with hydrothermal material (wollastonite, calcite, prehnite, pectolite, analcime). The latest step of pegmatite evolution corresponds to the development of bright green fringes, apophyses and cross-cutting veinlets, with a more-or-less aegirine-rich composition, on the pre-existing, commonly idiomorphic crystals of clinopyroxene. At their outermost rim, a brown color observed at some places corresponds to Ti-bearing aegirine. The only prominent accessory mineral is titanite.

Within the border region, the last change observed, at a few centimeters of the typical endoskarn boundary, is the disappearance of magnetite along a sharp front.

Thermobarometry

Crystallization temperatures are provided by the compositions of coexisting plagioclase and K-feldspar (CH2, UCV21). Assuming that the An content of the two feldspars has not re-equilibrated, temperatures were calculated according to the model for ternary feldspars of Green & Usdansky (1986) (Fig. 3). Good agreement is observed between measured and calculated compositions of coexisting phases, except for the Or content of the plagioclase, which is systematically lower than anticipated from calculation, most probably as a result of later K–Na exchange with the surrounding K-feldspar (Table 3). Such later exchange is not surprising, owing to the very small size of the plagioclase inclusions imbedded in K-feldspar in the "syenite" (sample CH2). In the "syenite", the observed pairs of coexisting feldspars crystallized from 820°C down to 760°C, and mostly around 790–800°C. In the case of the more internal part

TABLE 3. MEASURED AND CALCULATED* COMPOSITIONS OF COEXISTING FELDSPARS IN MONZODIORITE, CORNET HILL, ROMANIA

CH2	K-feldspar		Plagioclase	
	#4/57	Calc.	#4/56	Calc.
Ab %	33.5	34.22	75.3	67.56
Or %	64.4	63.70	2.10	9.64
An %	2.08	2.08	22.6	22.80

* See text.

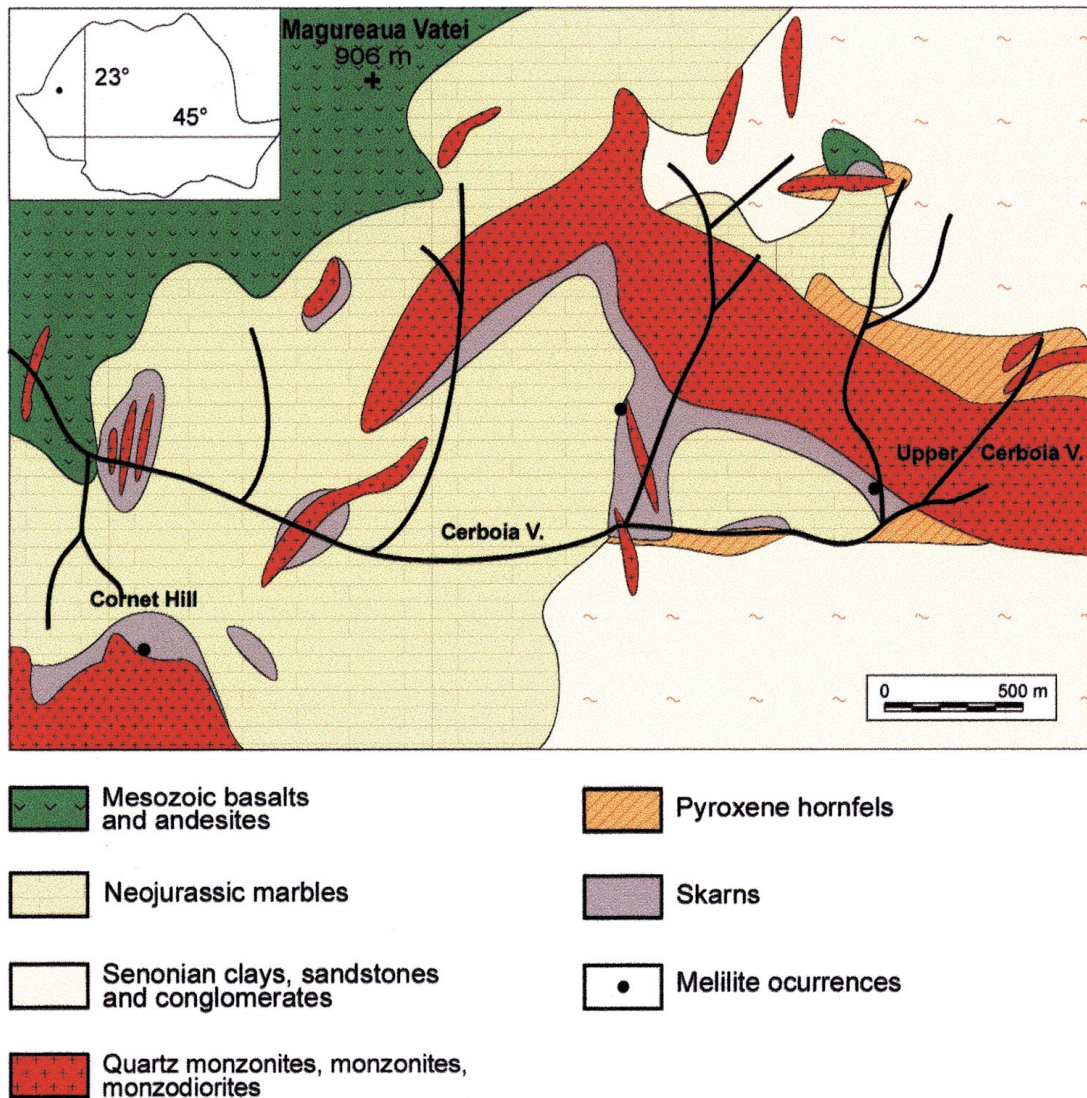


FIG. 1. Geological sketch of the Cerboia Valley region (redrawn from Stefan *et al.* 1978).

of the intrusion at UCV, crystallization temperatures in the range 800–740°C have been obtained.

In this temperature range, hornblende is stable at an H₂O pressure down to 0.5 kilobar (Burnham 1979). Whereas this mineral has been observed as early phenocrysts in the monzodiorite at CH, it only appears in very small amount at UCV, as probable remnants, almost entirely transformed to clinopyroxene. The monzodiorite plutons were thus emplaced in a shallow environment, with a H₂O pressure slightly higher at CH than at UCV, both being around 0.5 kilobar.

PARAGENETIC DESCRIPTION OF THE ZONED SKARNS

The changes in the intrusive rock are described from the endoskarn – “syenite” boundary outward, and will be followed by a description of the melilite veins and exoskarms. Zone A is composed of several subzones that may or may not be present in a given sample.

Zone A1

The endoskarms are demarcated by a very clear contact-parallel plane, which constitutes the first skarn front

TABLE 4. SELECTED COMPOSITIONS OF PYROXENE IN "SYENITE" AND SKARNS OF CORNET HILL AND UPPER CERBOAIA VALLEY, ROMANIA

Sample	"Syenite"			Zone A		Pyroxene veins in marble			
	CH2 Pl- bearing	CH78 Pl- free	CH78 zone A2	UCVZ Cpx relic inWo vein- let	late Cpx	with Grt	UCV4-1 with Grt	with Spl	with Cal
	4/60	10/54	10/43	10/23	10/27	4/45	1/41	1/18	1/2
SiO ₂ wt%	54.30	52.50	52.61	38.26	54.99	39.18	40.45	42.28	45.45
TiO ₂	0.09	0.36	0.23	2.36	0.07	1.18	0.92	0.50	0.64
Al ₂ O ₃	0.50	0.43	3.49	17.25	0.38	17.60	16.45	14.34	10.01
FeO	5.00	10.29	0.51	8.51	1.43	7.61	7.03	6.34	4.83
MgO	14.82	11.87	16.74	8.46	17.36	8.58	9.60	11.02	12.80
MnO	0.21	0.33	0.00	0.10	0.00	0.00	0.16	0.00	0.00
CaO	23.84	22.60	25.77	25.33	26.18	24.73	25.29	24.78	25.86
Na ₂ O	0.37	0.43	0.01	0.00	0.00	0.06	0.04	0.06	0.04
Total	99.13	99.81	99.36	100.27	99.41	99.20	99.93	99.33	99.63
Structural formulae for 6 O; Fe ²⁺ /Fe ³⁺ calculated for 4 cations, where possible									
Si <i>apfu</i>	2.010	1.961	1.911	1.424	1.984	1.469	1.500	1.569	1.679
Al	0.022	0.019	0.149	0.756	0.016	0.777	0.719	0.627	0.436
Fe ³⁺	0.000	0.142	0.016	0.264	0.012	0.223	0.218	0.197	0.149
Ti	0.003	0.010	0.006	0.066	0.002	0.033	0.026	0.014	0.018
Fe ²⁺	0.157	0.183	0.000	0.004	0.032	0.018	0.000	0.000	0.000
Mg	0.818	0.666	0.913	0.472	0.941	0.480	0.531	0.610	0.705
Mn	0.007	0.010	0.000	0.003	0.000	0.000	0.005	0.000	0.000
Ca	0.947	0.906	1.004	1.011	1.013	0.996	1.004	0.986	1.023
Na	0.027	0.103	0.001	0.000	0.000	0.004	0.003	0.004	0.003
Ecations	3.991	4.000	4.000	4.000	4.000	4.000	4.006	4.007	4.013

* From electron-microprobe analysis.

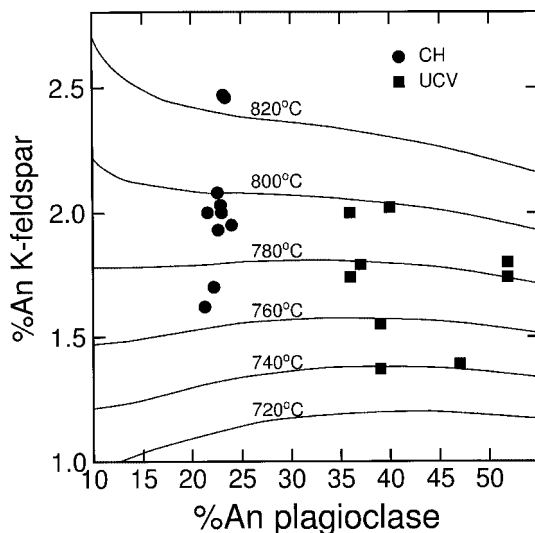


FIG. 3. An contents of coexisting alkali feldspar and plagioclase in syenite CH2 (dots) and monzodiorite UCV21 (squares). Isotherms calculated from Green & Usdansky (1986).



FIG. 2. Hand specimen of a melilite vein (BV) from UCV, sequence W, cross-cutting the wollastonite exoskarn. The beige mineral is a single crystal of wollastonite (10 cm in length). Idiomorphic black titanian garnet occurs between wollastonite and melilite (dark grey with white alteration). Yellow vesuvianite appears in the center of the patches of altered melilite (white).

in contact with the "syenite" (Fig. 4A). In the intrusive rock along the contact, a calcic mineral with a zeolite-like organization and a composition $\text{Na}_{0.10}\text{Ca}_2\text{Al}_{1.10}\text{Si}_3\text{O}_9.70(\text{H}_2\text{O})$ was observed, with a thickness up to 5 mm.

The pyroxene is idiomorphic and zoned, with the same grain-size and overall shape as in the intrusive rock, but with a different aspect (CH78). The rim progressively loses its shape and color, and becomes sieve-like. In other cases, a rim of fibrous wollastonite with fibers parallel to the pyroxene boundary develops at its expense. In some instances, it shows outer zones of intense green color, but interrupted and surrounded by wollastonite. Its composition (Table 4) shows changes in Fe and Na contents from the typical values in the "syenite" (1–10 wt.% FeO, 0.1–1.6% Na₂O, 4.5–0.4% Al₂O₃), to values that compare with those in zone A2 (less than 2% FeO, less than 0.1% Na₂O, 1.5–6% Al₂O₃).

Wollastonite is abundant and mainly occurs as subparallel fibers perpendicular to the contact, orga-

bution inherited from the intrusive rock have compositions in the range 5.0–9.5 wt.% Al_2O_3 and 0.17–1.24% TiO_2 (CH6, CH8). Later-formed very small grains of diopside (0.4–3.5 wt.% Al_2O_3 and less than 1.24% TiO_2) occur as scattered aggregates.

The garnet composition is Gr_{80-94} with less than 0.60 wt.% TiO_2 (Table 5, Fig. 5). A few aggregates of garnet (CH78, CH8) have a size and rectangular shape reminiscent of the idiomorphic plagioclase observed in

the monzodiorite (but not in the “syenite”). They are much more scattered and sporadic than the plagioclase of the main part of the intrusion, and may correspond to phenocrysts. In one case, a blurred zonation with a concentric idiomorphic outline was observed in this type of pseudomorph, which may be interpreted as being derived from a more sodic zone within this magmatic plagioclase.

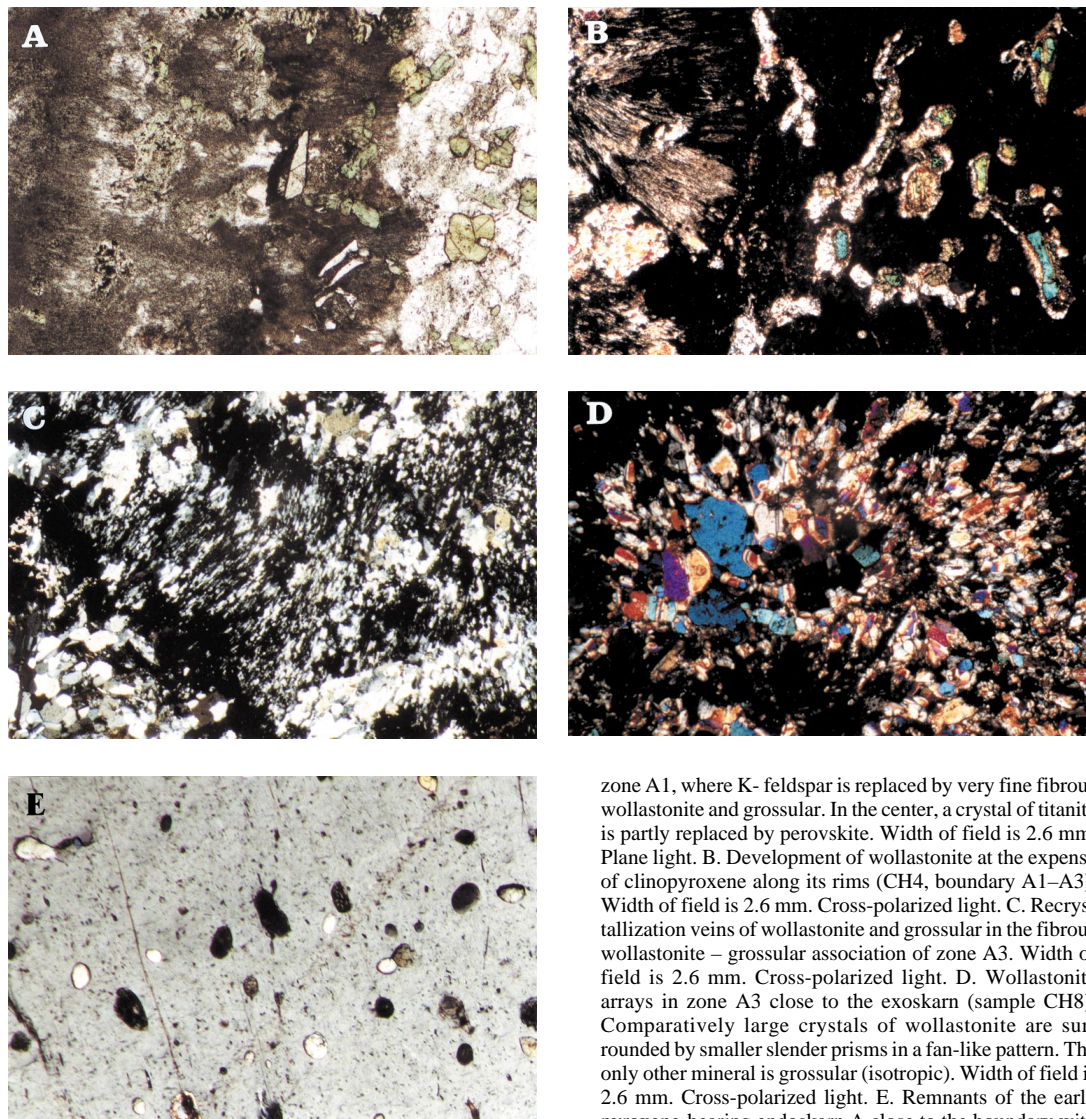


FIG. 4. Photomicrographs of zone A of the endoskarn. A. Boundary between the syenite on the right-hand side (K-feldspar, green clinopyroxene, titanite) and the endoskarn,

zone A1, where K-feldspar is replaced by very fine fibrous wollastonite and grossular. In the center, a crystal of titanite is partly replaced by perovskite. Width of field is 2.6 mm. Plane light. B. Development of wollastonite at the expense of clinopyroxene along its rims (CH4, boundary A1–A3). Width of field is 2.6 mm. Cross-polarized light. C. Recrystallization veins of wollastonite and grossular in the fibrous wollastonite – grossular association of zone A3. Width of field is 2.6 mm. Cross-polarized light. D. Wollastonite arrays in zone A3 close to the exoskarn (sample CH8). Comparatively large crystals of wollastonite are surrounded by smaller slender prisms in a fan-like pattern. The only other mineral is grossular (isotropic). Width of field is 2.6 mm. Cross-polarized light. E. Remnants of the early pyroxene-bearing endoskarn A close to the boundary with zone B (sample UCVZ). The light-colored rounded grains are aluminian diopside, the dark ones are grossular, all included in a large crystal of wollastonite. Width of field is 0.65 mm. Cross-polarized light.

Zone A2 may be almost indistinct, as in sample CH4, in which the green pyroxene inherited from the intrusive rock shows a transformation into wollastonite aggregates progressing along its margins (Fig. 4B). Diopside is only very sporadically observed in this sample, invariably as tiny grains.

Zone A3

Wollastonite and isotropic garnet are the predominant phases. Near the contact with zone A2, the fine fibrous, parallel texture of wollastonite typical of zone A2 is still present, and the garnet (Grs₉₅) is fine-grained, except for sporadic recrystallized patches (Fig. 4C). Further from the A2–A3 contact, recrystallized areas predominate, and wollastonite occurs as coarser more-or-less parallel prisms, but also as large xenomorphic patches, associated with grains of garnet of similar size and shape. The garnet composition is Grs₈₃ with 0.7–0.8 wt.% TiO₂. No perovskite could be found either in this zone or in A2.

In sample CH8, in the part of zone A3 nearest (5 mm) the exoskarn, a definite change is observed in the original texture of the rock: the slender prisms of wollastonite which, in this region, play the role of the

fibers of zone A1, are no longer parallel, but rather organized in fan-like pattern (Fig. 4D). The fan hinges are invariably oriented toward the marble. It is interesting to observe this texture in zone A (but *near the exoskarn*, in this sample and in CH22), because it is the one we find (with minor variants) in zone B.

In UCV 60 and 61, where the wollastonite – grossular association does not show any parallel orientation, a yellow titanian garnet (Table 5, Fig. 5) occurs in patches, associated with coarsely recrystallized wollastonite.

The boundary A–B

This boundary is rarely observed. One exception is sample CH8, in which zone A3 is in contact with zone B (somewhat modified). Another one is the wollastonite – garnet – vesuvianite association of sample UCVZ, in which wollastonite occurs as fan-like aggregates of slender prisms, associated with subordinate irregular small grains of colorless garnet (Grs₅₀). The garnet and vesuvianite crystals include a multitude of very small ghost crystals, commonly with a distinct rectangular outline, similar to what is commonly observed to remain of former clinopyroxene crystals in many garnet skarns. In a recrystallization vein, a large crystal of wollasto-

TABLE 5. SELECTED COMPOSITIONS OF GARNET FROM SKARNS OF CORNET HILL AND UPPER CERBOAIA VALLEY

	Early		Titanian				Spines		Late		Zone A				
	UCV4-16	ICH51-3/20	UCV9-10/16	CH49-5/7	CH3-14/21	UCV6-17	UCV9-14/38	UCV9-10/10	CH51-3/15	CH51-4/26	CH49-4/8	CH3-4/29	CH57-2/14	CH78-42/10	CH78-52/10
Cpx	incl.	relic	includes	zone	exo-	zone	between	vein-	contact	with	zone	zone	zone	zone	zone
veins	in Mel	in Wo	in Spu,	Wo	BV	skarn	A3	Mel	lets	with	Ves	Ves	A3	A2	
zone	zone	* assoc.	and			zone	rim of	zone	zone	Mel/	(alt.	(alt.			
	BV	Mel	Mel			C	crystal	BV	BV	Ves	Mel)	Mel)			
SiO ₂ , wt%	39.02	38.09	39.23	35.92	30.55	30.26	35.10	35.32	36.51	30.80	38.53	38.11	38.42	38.90	39.97
TiO ₂	0.36	0.09	0.84	3.14	8.11	9.31	4.02	4.10	0.03	6.27	1.27	1.29	1.88	0.72	0.09
Al ₂ O ₃	13.93	12.73	17.13	7.78	6.01	5.49	9.82	11.46	7.49	4.89	11.75	13.86	14.49	18.36	21.04
FeO (total)	9.94	12.38	7.11	17.51	18.69	19.75	14.03	12.20	18.99	20.05	13.29	9.64	7.64	4.82	1.74
MgO	0.41	0.12	0.56	0.37	0.58	0.65	0.61	0.14	0.08	0.37	0.21	0.30	0.43	0.53	0.07
MnO	0.04	0.00	0.13	0.00	0.04	0.02	0.08	0.01	0.12	0.04	0.00	0.05	0.00	0.06	0.19
Cr ₂ O ₃	n.a.	0.00	n.a.	n.a.	0.05	0.10	0.00	n.a.	0.04	0.28	0.18	0.00	n.a.	n.a.	n.a.
CaO	35.37	35.53	36.52	35.55	34.15	33.84	34.08	35.41	33.93	32.96	35.83	36.09	35.74	36.06	36.51
Na ₂ O	0.00	0.01	0.01	0.00	0.02	0.00	0.00	0.01	0.00	0.00	0.01	0.00	0.00	0.03	0.00
Total	99.07	98.95	101.53	100.27	98.20	99.42	97.76	98.73	97.19	95.66	101.07	99.34	98.60	99.50	99.61
Structural formulae for 12 O; Fe ²⁺ /Fe ³⁺ calculated for 8 cations															
Si <i>apfu</i>	3.028	2.988	2.958	2.855	2.529	2.475	2.833	2.807	2.978	2.614	2.972	2.968	3.002	2.973	3.019
Al	1.436	1.177	1.521	0.729	0.585	0.529	0.934	1.073	0.720	0.489	1.068	1.272	1.334	1.653	1.872
Fe ³⁺	0.535	0.822	0.454	1.165	1.298	1.367	0.916	0.814	1.311	1.440	0.867	0.635	0.446	0.312	0.111
Ti	0.021	0.005	0.048	0.187	0.505	0.573	0.244	0.245	0.002	0.401	0.074	0.076	0.110	0.041	0.005
Fe ²⁺							0.042						0.059		
Cr				0.003	0.006	0.000		0.003	0.018	0.011					
Mg	0.047	0.014	0.063	0.044	0.072	0.080	0.073	0.017	0.010	0.047	0.024	0.035	0.050	0.061	0.008
Mn	0.003	0.0	0.008	0.0	0.003	0.001	0.005	0.006	0.008	0.003	0.0	0.003	0.0	0.004	0.012
Ca	2.941	2.991	2.954	3.032	3.029	2.969	2.952	3.037	2.969	3.000	2.965	3.015	2.997	2.957	2.959
Na	0.000	0.001	0.001	0.000	0.003	0.000	0.000	0.001	0.000	0.000	0.001	0.000	0.000	0.004	0.000

From electron-microprobe analysis. * In Wo – Cpx – Grs zone.

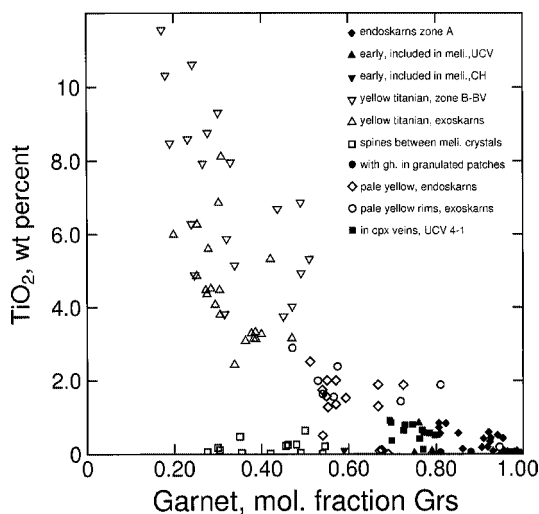


FIG. 5. Compositions of garnet from CH and UCV skarns.

nite was found to contain numerous minute rounded (but neither altered nor corroded) inclusions (Fig. 4E), probably preserved as armored relics, among which pyroxene is predominant. This pyroxene contains 49 to 54 mol.% of the $\text{Ca}(\text{Al,Fe})_2\text{SiO}_6$ end-member and also comparatively high Ti contents (e.g., #10/23, Table 4). At a distance of 2 cm, one small grain of melilite (#10/17, Table 6) and idiomorphic grains of grossular (Gr_{57} , 0.84 wt.% TiO_2) were found as inclusions in other crystals of wollastonite. The presence of relics of melilite, aluminian diopside and grossular in this rock suggests that it contained, prior to the development of the association vesuvianite – wollastonite – garnet, the boundary between the zone B and a zone resembling A2, although the pyroxene has a peculiar, Al-rich composition.

Zone B

Zone B is composed of wollastonite and melilite in comparable amounts and in apparent equilibrium. In this zone and in the coarse-grained melilite vein described below, the composition of melilite shows little variation: 57–65 mol.% Gh with X_{Mg} in the range 0.82–0.89 (Table 6, Fig. 6). At UCV, it is more Na-rich (4.3 to 6 mol.% “Na-melilite”) than at CH (1.8 to 3.1 mol.% “Na-melilite”).

In sample UCV8, melilite occurs mostly as rather small crystals of almost uniform size with a certain idiomorphic tendency, without any observable zoning. Wollastonite occurs as short prisms, of the same size as the associated crystals of melilite, commonly with a more-or-less parallel orientation. However, from place to place, melilite shows a striking tendency to an organization in parallel grains that tend to coalesce into

porphyroblasts with a diameter at least ten times larger than the individual grains (Fig. 7A). These randomly distributed porphyroblasts constitute an important fraction of the rock, and contain numerous very small rounded crystals of wollastonite.

At CH, a mosaic association of melilite and wollastonite is observed, with a weak but distinct orientation of the wollastonite prisms as in UCV8. However, wollastonite also shows another type of textural development, reminiscent of that found in zone A3 (CH8) or A2 (CH22): radiating circular arrays of relatively short slender prisms, organized around large patches formed of one or a few crystals with a good development of faces ($h0l$). Melilite tends to segregate or to constitute short blind veins, and the mosaic texture is interrupted by a network of veins of very coarsely crystallized wollastonite \pm melilite (Fig. 7B). In CH8, the narrow (less than 5 mm) zone B, in contact with the fibrous garnet – wollastonite association of zone A3, consists of predominant coarse melilite (entirely replaced by an aggregate of Al-rich vesuvianite) associated with very coarse, stout prisms of wollastonite.

The wollastonite near the exoskarn boundary is resorbed owing to the corrosion of the large patches, or their persistence only as small rounded inclusions in melilite crystals of uniform size (0.5 mm, CH10, CH12, CH13). This is perhaps also the case in CH49, in which wollastonite occurs as rare clusters of tiny interlocking

TABLE 6. SELECTED COMPOSITIONS OF MELILITE AND “BICCHULITE” FROM SKARNS AT CORNET HILL AND UPPER CERBOAIA VALLEY, ROMANIA

	CH51 1/73c core	CH51 1/71b rim	CH49 1/61c core	CH49 1/62b rim	CH49 5/16 incl. in Ves	CH49 8/18 incl. in “Bcl”	UCVZ 10/17 incl. in Wo	UCV8 48
SiO_2 wt%	29.14	30.15	26.58	26.72	25.80	23.72	30.32	31.09
TiO ₂	0.04	0.03	0.00	0.00	0.00	0.00	0.01	0.00
Al ₂ O ₃	24.12	23.03	28.05	27.23	30.46	27.29	22.27	21.20
Cr ₂ O ₃					0.06	0.00		0.02
FeO	1.88	1.66	0.62	0.76	0.30	0.34	2.02	1.64
MgO	3.88	4.34	3.13	3.03	2.34	4.36	4.20	4.81
MnO	0.09	0.04	0.00	0.15	0.11	0.03	0.04	0.04
CaO	39.97	40.05	40.25	40.33	41.01	36.91	40.37	40.38
Na ₂ O	0.31	0.35	0.20	0.20	0.22	0.22	0.05	0.61
K ₂ O	0.00	0.00	0.00	0.02	0.00	0.00	0.00	0.05
Total	99.46	99.65	98.83	98.45	100.30	92.70	99.86	99.83
Structural formulae for 7 O								
Si <i>appu</i>	1.345	1.386	1.229	1.244	1.176	1.168	1.397	1.431
Al	1.312	1.247	1.528	1.495	1.636	1.583	1.209	1.150
Ti	0.001	0.001	0.000	0.000	0.000	0.000	0.000	0.000
Cr					0.002	0.000		0.001
Fe ²⁺	0.073	0.065	0.024	0.029	0.012	0.014	0.079	0.063
Mg	0.267	0.297	0.216	0.211	0.159	0.322	0.291	0.330
Mn	0.002	0.001	0.000	0.006	0.004	0.001	0.002	0.002
Ca	1.980	1.976	1.996	2.013	2.006	1.950	1.996	1.976
Na	0.028	0.031	0.018	0.018	0.019	0.005	0.056	0.055
K	0.000	0.000	0.000	0.001	0.000	0.000	0.000	0.003

From electron-microprobe analyses. Bcl: bicchulite.

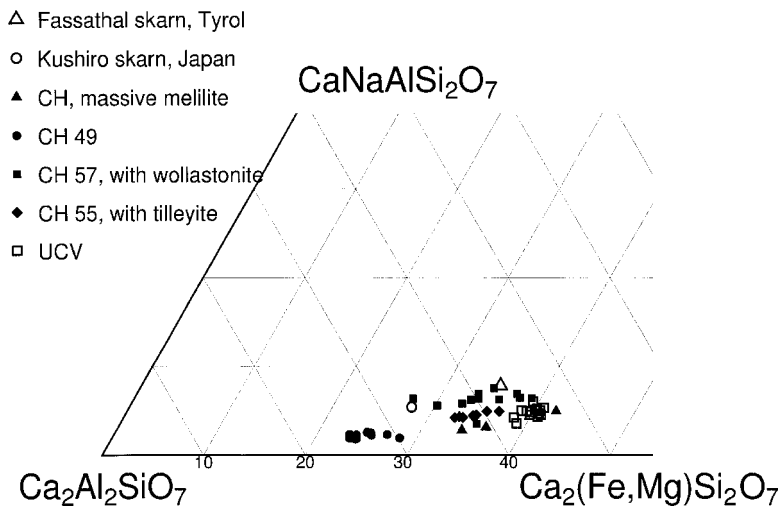


FIG. 6. Compositions of melilite of the vein stage (mol. fraction) in skarns from CH and UCV (this study), and other skarns (as given by Deer *et al.* 1986).

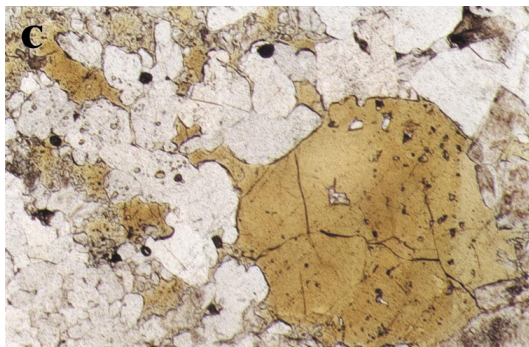
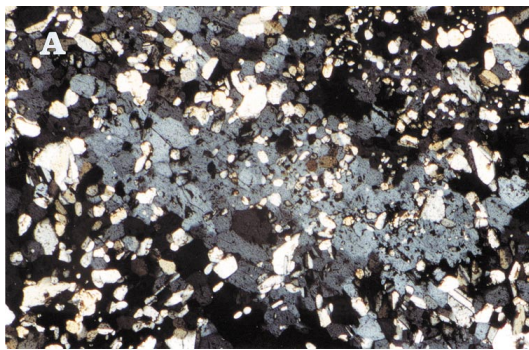


FIG. 7. Photomicrographs of zone B of the endoskarn. A. Coalescence of the melilite crystals (bluish grey) into porphyroblasts that include wollastonite crystals of smaller size than wollastonite not included in melilite. Width of field is 2.6 mm. Cross-polarized light. B. Wollastonite array similar to that of zone A3 (Fig. 4D). Melilite occurs as veins on the right-hand side. The isotropic mineral around and in the outer part of the "cauliflower" is titanian garnet. Width of field is 2.6 mm. Cross-polarized light. C. Rounded idiomorphic crystal of titanian garnet, extended by interstitial veinlets between melilite crystals ("spines"). Width of field is 2.6 mm. Plane light.

grains with no tendency to elongate shapes and no apparent twinning and, in some cases, as inclusions in melilite in the vicinity of the clusters.

The only other mineral observed in these rocks (apart from secondary veins) is titanian garnet. Its most spectacular mode of occurrence is as large yellow crystals,

either as poikilitic patches similar to those mentioned in zone A3, developed on sectors of the circular wollastonite arrays (Fig. 7B) and in the wollastonite veins, or as rounded grains (Fig. 7C) with inclusions of wollastonite and melilite. The garnet composition is in the range Grs₂₆₋₃₅, with 5.22–8.11 wt.% TiO₂ (Table 5, #14/21).

Granules of pyrrhotite (CH3, CH51) or pentlandite (CH3) (or both) are common, but occur in small amounts; perovskite is rarely observed as tiny octahedra.

From this point on, there are differences between sequences S and W, which are thus described separately.

Sequence W: vein BV

The contact of zone B (UCV8) with the melilite vein BV is sharp and characterized by textural changes in melilite and by the fact that wollastonite loses any trace of subparallel orientation (Fig. 8A). Textural changes in the melilite crystals include a larger average grain-size, an extreme variability in grain-size (0.2 mm –

5 cm), and a striking idiomorphic character. In places, but less commonly than in zone B, a tendency toward near-parallelism and coalescence of smaller crystals is observed. A pattern of very fine lamellae of magnetite in two or three orientations occurs locally in the core of the melilite crystals, with a very regular and uniform distribution that suggests an exsolution origin, but it is only exceptionally and locally observed in the rim (Fig. 8B).

In UCV8, wollastonite disappears after a 1-mm-wide zone, where it recrystallizes in large poikilitic amoeba-like patches, replaced by calcite or, less commonly, brownish yellow garnet (Grs₃₁, 10.4 wt.% TiO₂) up to the boundary of the wollastonite zone. From place to place within a few millimeters of this boundary, remnants of poikilitic interstitial coarse wollastonite are included in calcite or yellow garnet. This garnet especially occurs in contact with zone C, either as individual crystals (Fig. 8C) or as an almost continuous fringe (UCV65; Fig. 2B).

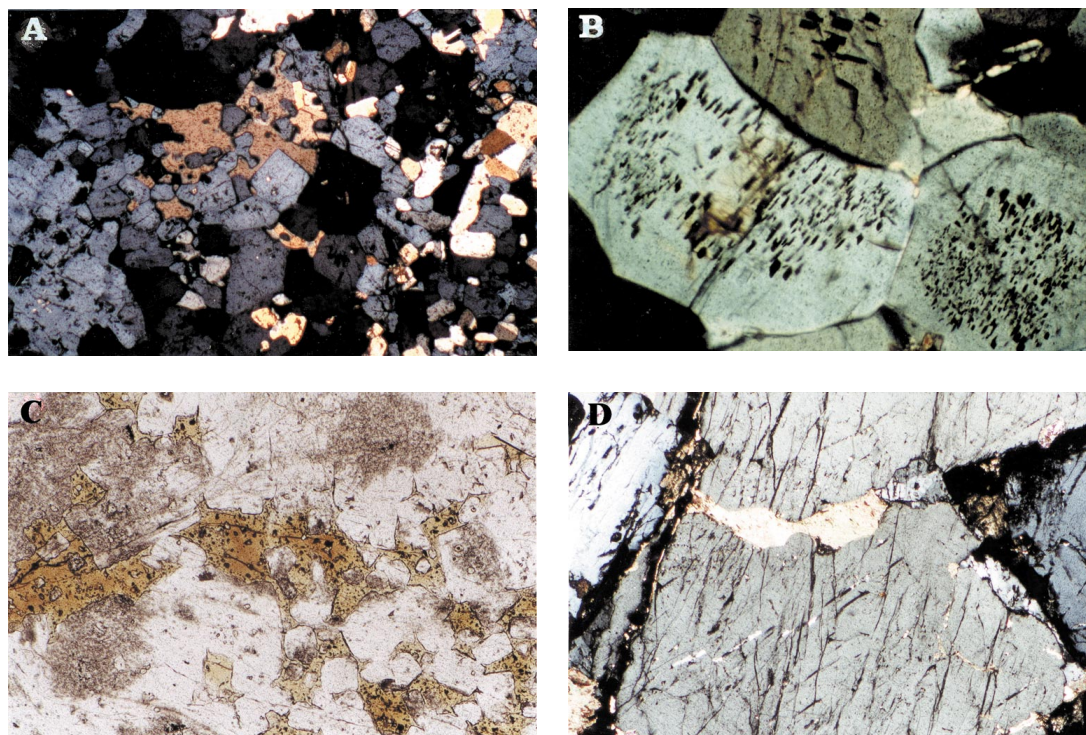


FIG. 8. Photomicrographs of the melilite veins (BV) at UCV, sequence W. A. Boundary between zones B (right) and BV (left). Melilite crystals (bluish grey) change to a larger size and idiomorphic shape, and wollastonite (yellow and light-colored) becomes poikilitic, then disappears. Width of field is 2.6 mm. Cross-polarized light. B. Magnetite lamellae in the core of weakly zoned crystals of melilite. Width of field is 1.2 mm. Cross-polarized light. C. Interstitial brownish yellow titanite garnet, enclosing idiomorphic crystals of melilite, and extended by paler veinlets ("spines"). The greyish dotted patches in melilite are described as the granular modification. Width of field is 2.6 mm. Plane light. D. Veinlet of calcite and hydroxyllellastadite (light grey) between melilite and wollastonite and cross-cutting wollastonite. Width of field is 2.6 mm. Cross-polarized light.

Veinlets of P-rich hydroxyllellestadite associated with calcite have been observed along the boundary BV – C with a short cross-cutting extension in the wollastonite (Fig. 8D). In UCV65, the texture suggests that the veinlets formed before the titanian garnet.

Sequence W: zone C

Any relation with the endoskarn texture is lacking. Zone C is characterized by very large (more than 2 mm, commonly several centimeters) idiomorphic prisms of wollastonite that mould the adjacent crystals of melilite of vein BV, but do not penetrate in the intergranular spaces between the melilite crystals, invariably filled with calcite. Wollastonite is partly corroded by calcite patches along its cleavages, especially near the boundary BV – C. Further from this boundary, calcite is observed in the interstices of the wollastonite framework. The titanian garnet is also observed in the zone C near the boundary BV – C (Table 5, #14/38), partly replacing wollastonite and the associated corroding calcite. In all cases, the crystals are zoned, and their titanium and iron contents decrease from center to rim (*e.g.*, UCV7, Grs_{44–49} with 6.7–5.0 wt.% TiO₂; UCV6, Grs_{30–42} with 9.3–5.3% TiO₂).

Sequence S: vein BV

At CH, the vein composed of melilite with a uniform grain-size (0.5–1.5 mm) is separated from the much finer-grained zone B by a regular planar surface, and it may be a few millimeters thick (CH30, CH8; Fig. 9A), or constitute the whole of a thin section (CH51). In this sample, the idiomorphic crystals of melilite show a growth zonation without appreciable compositional change, and the same inclusions of magnetite lamellae as described in sequence W. They include granules of perovskite in their rim (rarely) and of hydroxyllellestadite along their boundaries. The composition of hydroxyllellestadite shows small variations (Table 7). It is PO₄-poor and has an atomic ratio S:Si less than 1, attributed to the presence of CO₃ substituting for SO₄. An early grossular-rich garnet (Grs₅₉; Table 5, #3/20) observed as an inclusion in a melilite crystal provides our only information on the composition of the garnet present in the rock at the time of melilite crystallization.

Narrow veinlets, strings or groups of small idiomorphic crystals of melilite, rooted in the main vein, occur in the first few centimeters of zone C. In CH30, the melilite veinlets develop (with the same grain-size as in the main vein) either alone (Fig. 9B) or in association

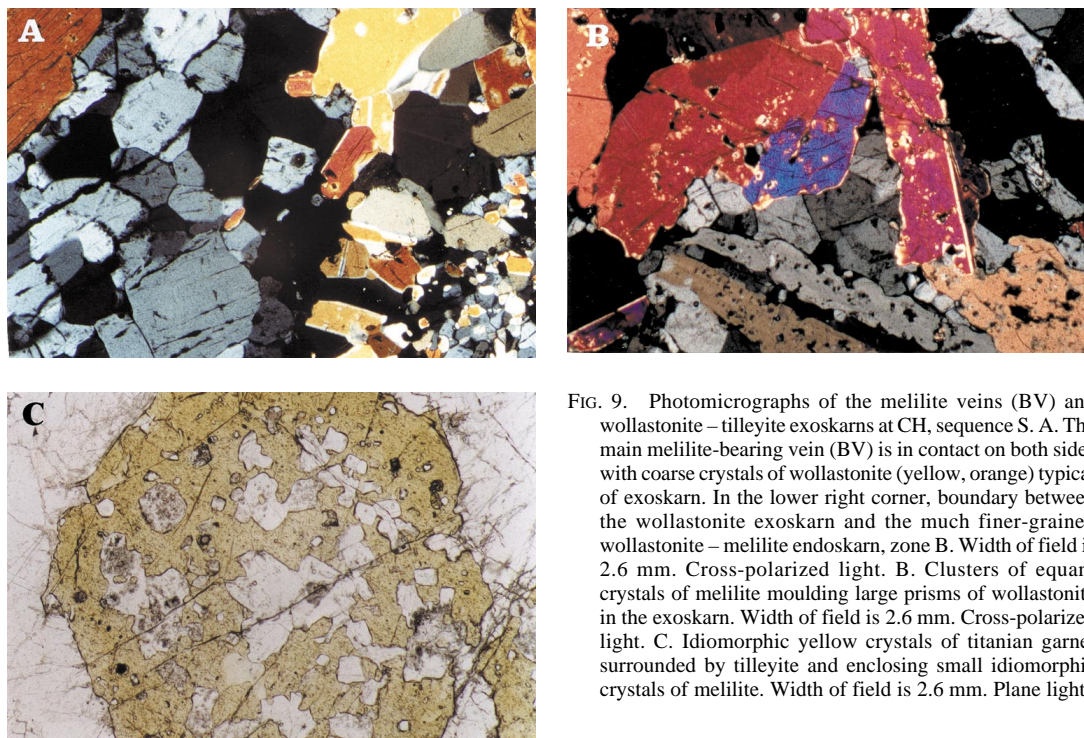


FIG. 9. Photomicrographs of the melilite veins (BV) and wollastonite – tilleyite exoskarns at CH, sequence S. A. The main melilite-bearing vein (BV) is in contact on both sides with coarse crystals of wollastonite (yellow, orange) typical of exoskarn. In the lower right corner, boundary between the wollastonite exoskarn and the much finer-grained wollastonite – melilite endoskarn, zone B. Width of field is 2.6 mm. Cross-polarized light. B. Clusters of equant crystals of melilite moulding large prisms of wollastonite in the exoskarn. Width of field is 2.6 mm. Cross-polarized light. C. Idiomorphic yellow crystals of titanian garnet surrounded by tilleyite and enclosing small idiomorphic crystals of melilite. Width of field is 2.6 mm. Plane light.

with much larger crystals of tilleyite in all possible interstitial (calcite-filled early on) spaces between the large prisms of wollastonite in the exoskarn, which show recrystallization along their margins. At a distance of 1 cm, the apophyses of the vein on the exoskarn side change into veinlets and clusters. In CH8, in the same situation, melilite constitutes a dense irregular network of large idiomorphic crystals, replaced by vesuvianite.

The yellow titanian garnet (e.g., CH1, Grs_{17–25} with 11.5–4.88 wt.% TiO₂) partly replaces wollastonite and tilleyite. In this case, it has an irregular and ragged outline. It also occurs as comparatively large rounded crystals that include many small idiomorphic crystals of melilite and also wollastonite and tilleyite (Fig. 9C). One yellow garnet crystal (CH7, Grs₂₄, 10.6 wt.% TiO₂) is associated with a small aggregate of perovskite granules defining an idiomorphic outline, suggesting that perovskite could have replaced a titanite crystal.

Sequence S: the spurrite – melilite variant of vein BV

Sample CH49 is the only one composed mainly of the spurrite – melilite association. Melilite is finer grained and distinctly more Al-rich than usual (67–77 mol.% Gh, with X_{Mg} in the range 0.87–0.94; Table 6).

On the inner side, this association is separated from the wollastonite – melilite association by the association hydroxyllestadite – melilite, in which hydroxyllestadite (Table 7) occurs as very small crystals, commonly included in the rim of the melilite crystals.

In the outer part of the spurrite – melilite zone, spurrite and melilite seem in equilibrium. Their grain sizes are similar and very irregular. In the absence of deformation, large idiomorphic crystals of melilite in contact with spurrite show a texture similar to that described at the boundary BV – C at UCV. A distinct banding results from variations in their proportions, and this banding is confirmed by the distribution and clustering of very small but numerous grains of perovskite invariably included in the melilite bands (Fig. 10A).

Along the contact with zone C, there is evidence of a complicated process of deformation: the spurrite bands are folded, and the spurrite crystals are fragmented, and enclosed in undeformed tilleyite, neither showing any tendency of annealing. Short veinlets of idiomorphic melilite develop in the tension cracks (Figs. 10B, C). In one such veinlet, a small cluster of perovskite grains is included in the melilite. The main plane of deformation is followed on the inner side by a shear zone 5 mm thick, which contains part at least of the hydroxyllestadite-bearing assemblage. In this sheared zone, melilite is granulated and recrystallized into very small (0.1 mm) interlocking crystals, in the fashion of quartzite in low-grade metamorphism. Spurrite is also recrystallized as poikilitic porphyroblasts (0.5 mm), with a well-developed (001) face, commonly transverse to the shear plane.

Titanian garnet occurs around and at the expense of the perovskite granules in the banded part of the sample, and also in the perovskite-free sheared area, with a regular sieve-like pattern.

Sequence S: zones C and D

The massive spurrite zone and the tilleyite zone have been described by Istrate *et al.* (1978). The grain size of spurrite is variable and locally very large. The spurrite crystals are flattened and show a predominant development of face (001) and widespread polysynthetic twinning in the same direction. The other known twin plane, (101), is rarely observed and not polysynthetic. In sample CH1, coarse-grained tilleyite partly replaces spurrite, of which corroded remnants are preserved. In CH49, tilleyite appears along a calcite vein as a millimeter-thick fringe between calcite and spurrite (Fig. 10D). There is no evidence of spurrite – tilleyite incompatibility, but where mutual relationships were observed, tilleyite was found to form after spurrite and partly at the expense of this mineral (Fig. 10E).

In many samples, the exoskarn includes only a well-defined wollastonite – tilleyite zone, following either the zone B (CH20) or the vein BV (CH30). It contains veinlets of melilite and titanian garnet and large blades of wollastonite with a corroded outline. In CH8, stout prisms of wollastonite form a single row with a clear idiomorphic development toward the wollastonite – calcite – melilite association of the outer part of the exoskarn. Tilleyite is either preserved or replaced by a fine-grained secondary aggregate of calcite and wollastonite. The transition to the coarse-grained marble takes place with an idiomorphic relation of tilleyite toward calcite.

PARAGENETIC DESCRIPTION OF PYROXENE VEINS IN THE MARBLE

The calcite-free veinlets in sample UCV4–1 mainly consist of pyroxene, usually associated with garnet (Grs_{72–80} with 0.12–0.67 wt.% TiO₂, Table 5) or, in some cases, with a little green spinel (Mg_{0.91–0.86}Fe²⁺_{0.09–0.14}Al_{1.98}Fe³⁺_{0.02}O₄). Cl-bearing vesuvianite (#3/4 and 3/5, Table 8) appears as a narrow rim along some veinlet boundaries. It tends to change to garnet.

Calcite-bearing parts of the sample show regularly scattered grains of pyroxene similar to the ones in the calcite-free veinlets. Some of these pyroxene grains are enclosed in calcite, with a distribution in the outer parts of calcite crystals, showing that they mostly developed along the boundaries of calcite grains and that these boundaries were later displaced by calcite recrystallization. A few small crystals of spinel (Mg_{0.84}Fe²⁺_{0.16}Al_{1.91}Fe³⁺_{0.09}O₄) and of phlogopite (19–20 wt.% Al₂O₃, X_{Mg} 0.93–0.94), 10 μm in diameter, are enclosed in calcite or, more commonly, in the vicinity of the pyroxene.

The composition of the pyroxene strongly depends on the nature of its immediate neighbors. In veinlets or in direct contact with Al-bearing minerals (garnet, vesuvianite, spinel or phlogopite), it is aluminian diopside (13.5 to 19.4 wt.% Al_2O_3) with a variable Ti content, up to 2.6 wt% TiO_2 , quite similar to the aluminian diopside observed as inclusions in the endoskarn UCVZ (Table 4, Fig. 11). Where in direct contact only with calcite, the pyroxene has a variable but lower content Al content. According to the inferred structural formula, all iron is trivalent, and the ratio $\text{Fe}^{3+}:\text{Al}$ (0.31), approximately constant, corresponds to almost equal mole fractions (up to 28%) of esseneite and CaTs components. This constant ratio is interpreted as due to the occurrence of pyroxene in equilibrium with a garnet of almost constant composition (Grs_{72-80}), owing to the reciprocal equilibrium between CaTs, esseneite, grossular and andradite (Table 9, eq. 46).

PARAGENETIC DESCRIPTION OF SECONDARY MODIFICATIONS

The monticellite-bearing granular modification of melilite

A granular type of modification of melilite occurs as rounded patches, commonly with sharp outlines, along almost indistinct fractures in the zone BV (Figs. 8C, 12A). A veinlet of this type has been observed to cross the recrystallization boundary (CH8) in only in one case. Near the contact of the zone BV with the wollastonite exoskarns at UCV, the patches are larger and coalescent, and the portions of melilite in contact with the wollastonite (and calcite) exoskarns that persist without modification of this type are scanty. Toward the inside of zone BV, this outer part extends as delta-shaped zones of more localized alteration in continuity with the veinlets. At CH, smaller patches of a granular modification are observed in the melilite veinlets developed in the exoskarns.

The patches consist of melilite with the same orientation as the normal melilite outside, but having a higher birefringence; this melilite is associated with granules of monticellite, variable amounts of garnet, and some phases whose high birefringence and compositions indicate the CSH family. In one case, a mineral of rankinite composition (UCV8) was observed, but wollastonite was not found. Where such a veinlet crosses the amoeba-like patches of wollastonite, the wollastonite is mostly unaffected. Both melilite and garnet show progressive shifts toward Al-rich compositions, with increasing development of the modification, up to Gh₉₂ and Gr₈₈, respectively (UCV9). The granular areas show in some places a further evolution, with rounded centers of vesuvianite separated from the other minerals mentioned by a narrow rim of brownish, poorly crystallized phyllosilicate-like material.

TABLE 7. SELECTED COMPOSITIONS OF HYDROXYLELLESTADITE FROM SKARNS AT CORNET HILL, ROMANIA

	CH49* 1/8	CH49* 1/17	CH51 2/30	CH51 2/34
SiO ₂ wt%	17.71	17.10	15.62	19.29
TiO ₂	0.04	0.00	0.01	0.00
Al ₂ O ₃	0.06	0.04	0.01	0.02
P ₂ O ₅	3.38	3.94	4.80	1.21
FeO	0.32	0.05	0.07	0.00
MgO	0.01	0.01	0.01	0.04
MnO	0.12	0.00	0.04	0.01
CaO	58.15	57.28	56.33	57.96
Na ₂ O	0.26	0.26	0.25	0.31
K ₂ O	0.05	0.06	0.03	0.03
SO ₃	14.66	12.64	12.98	12.59
F	0.00	0.54	1.73	0.84
Cl	0.10	0.09	0.37	0.54
CO ₂ (calc)	4.71	5.36	5.27	5.33
H ₂ O (calc)	1.87	1.58	0.92	1.35
Total	101.34	98.70	97.63	99.15
Structural formulae on the basis of Ca + Mg + Mn + Fe + Al + Na + K = 10				
P	0.452	0.538	0.666	0.163
Si	2.796	2.755	2.560	3.066
S	1.737	1.529	1.597	1.501
C = 6 - Si - S - P	1.015	1.178	1.177	1.270
Al	0.012	0.008	0.001	0.004
Fe	0.042	0.006	0.010	0.000
Mg	0.003	0.003	0.002	0.010
Mn	0.016	0.000	0.006	0.002
Ca	9.837	9.891	9.893	9.869
Na	0.079	0.081	0.081	0.096
K	0.010	0.012	0.006	0.007
F	0.000	0.273	0.895	0.425
Cl	0.028	0.024	0.104	0.145

* Results of electron-microprobe analyses.

In sample CH51, a modification of the same type is developed as very narrow regions along a few fractures. The birefringence of melilite progressively increases, and small irregularly scattered granules of monticellite appear. These veinlets cross pre-existing spines of garnet (see below). At a few places along these veinlets, rounded spots of the more usual granular patches appear. One of them shows a center of grossular with a rim of melilite Gh₈₀₋₉₀ 80 μm wide and a few grains of cuspidine. Monticellite is observed at a distance of 0.2 mm. Monticellite alone, without compositional change of the adjacent melilite, occurs as independent veinlets (Fig. 12B). Magnetite and pyrrhotite (in some cases Ni-rich, tending to a pentlandite composition) occur sporadically in the same intergranular spaces as monticellite.

Garnet spines and veins, and vesuvianite in melilite-bearing rocks

Garnet regularly occurs as localized and limited networks of very thin discontinuous veinlets, called "spines" by Burnham (1959), which appear between melilite grains, and occasionally between melilite and

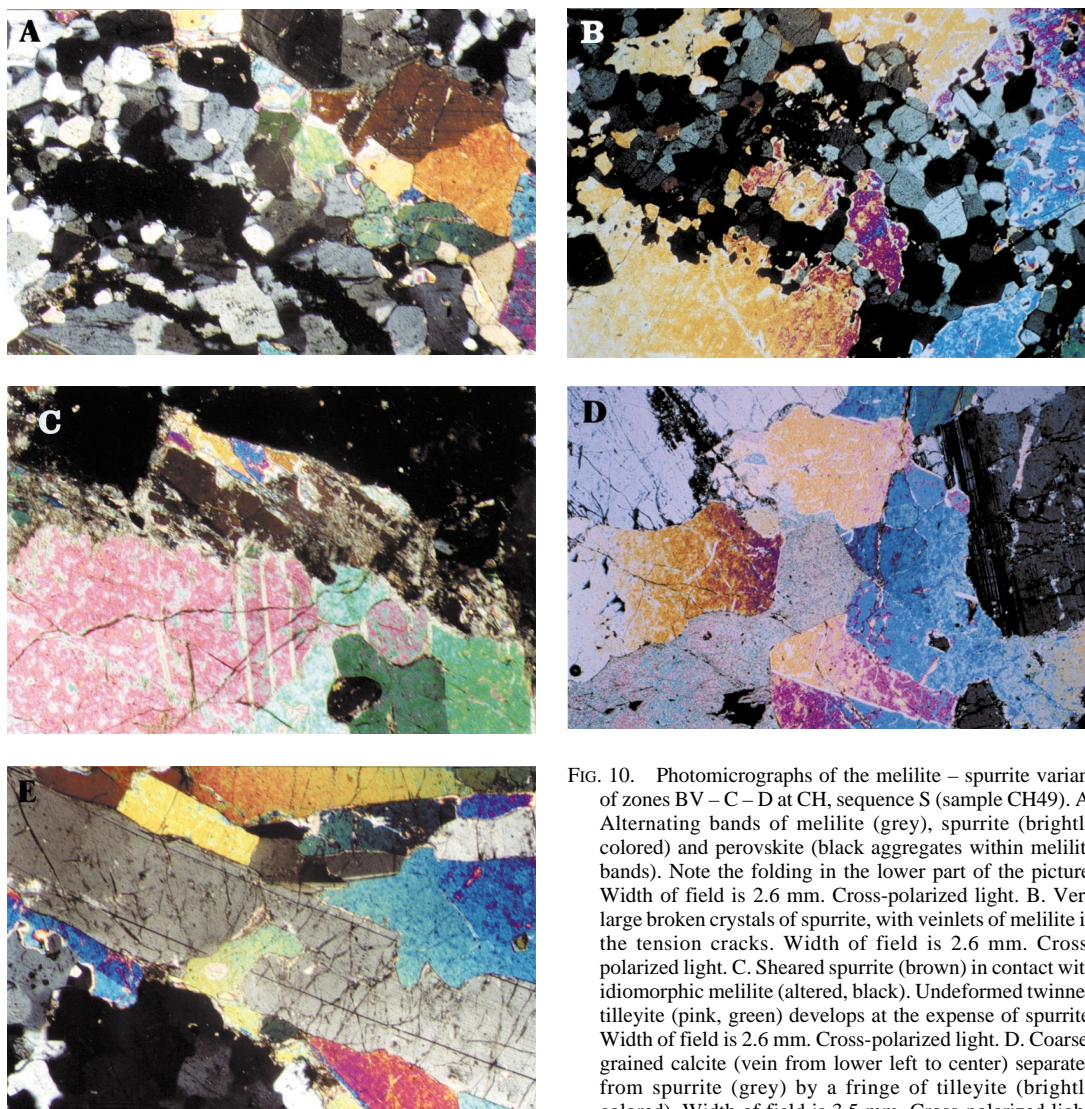


FIG. 10. Photomicrographs of the melilite – spurrite variant of zones BV – C – D at CH, sequence S (sample CH49). A. Alternating bands of melilite (grey), spurrite (brightly colored) and perovskite (black aggregates within melilite bands). Note the folding in the lower part of the picture. Width of field is 2.6 mm. Cross-polarized light. B. Very large broken crystals of spurrite, with veinlets of melilite in the tension cracks. Width of field is 2.6 mm. Cross-polarized light. C. Sheared spurrite (brown) in contact with idiomorphic melilite (altered, black). Undeformed twinned tilleyite (pink, green) develops at the expense of spurrite. Width of field is 2.6 mm. Cross-polarized light. D. Coarse-grained calcite (vein from lower left to center) separated from spurrite (grey) by a fringe of tilleyite (brightly colored). Width of field is 3.5 mm. Cross-polarized light. E. Elongate prisms of spurrite (grey) corroded and partly replaced by tilleyite (brightly colored). Width of field is 2.6 mm. Cross-polarized light.

wollastonite or tilleyite (but never spurrite), not related to the granular areas but occasionally enclosing them (Fig. 8C). In zone B of UCV8, they occur everywhere (Gr_{54} , with 1.33 wt.% TiO_2). In CH5 and CH57, part of the spines occur as crowns around the crystals of yellow garnet (Fig. 7D), with a regular compositional change from the centers of the garnet patches to the outer limit of the spines. They are also common in zone B of sequence S. In vein BV of UCV8, a similar garnet (Gr_{52-55} , 0.2–1.85 wt.% TiO_2) develops in interstitial spaces between melilite crystals, in an intermediate position between wollastonite and calcite or yellow

titanian garnet, forming a zone 3 mm wide parallel to the boundary B – C.

Closest to the spines, the magnetite lamellae included in the core of melilite crystals (UCV8, CH51) are commonly partially replaced by Ti-free garnet (Fig. 12B). Rounded granules of the same garnet (Gr_{42-65}) are commonly included in recrystallized wollastonite (UCV8).

In continuity with the spines, thin calcite–garnet veinlets in exoskarms (CH49, spurrite zone) are related

TABLE 8. SELECTED COMPOSITIONS OF VESUVIANITE FROM SKARNS AT CORNET HILL AND UPPER CERBOAIA VALLEY, ROMANIA

	Cpx veins		Boundary A-B			Boundary B-C			Alteration of melilite				
	UCV 4-1 3/4	UCV 4-1 3/5	CH49 4/15 contact with Mel	UCVZ 10/3 Wo- Grt- Ves	UCVZ 10/31 in Wo veins, rim	CH49 8/26 symp. Cal	UCV 7 15/8 exo- skarn tit. Grt	UCV 15 15/44 core same as 15.44, rim	UCV 15 15/42	CH57 2/10	CH57 2/12	CH49 8/17	CH7 37/49
SiO ₂ wt%	32.72	32.63	35.83	35.67	36.60	37.15	36.06	34.85	35.86	33.05	37.00	35.06	32.97
TiO ₂	0.03	0.02	0.68	0.05	0.04	0.18	1.84	0.01	0.18	0.00	0.07	0.06	0.01
Al ₂ O ₃	18.56	19.77	15.51	17.02	15.74	16.85	13.94	18.34	13.34	19.78	16.54	16.69	19.33
FeO	0.59	0.50	4.73	0.91	1.82	3.73	3.43	1.43	3.11	0.48	2.89	1.93	0.71
MgO	4.22	3.54	3.16	4.64	4.24	2.97	4.52	3.95	5.19	2.62	3.06	3.96	6.14
MnO	0.05	0.01	0.00	0.04	0.00	0.17	0.09	0.00	0.18	0.05	0.11	0.00	0.13
CaO	36.63	36.61	35.97	37.21	37.29	37.77	35.14	35.40	35.94	36.38	36.11	37.70	34.04
Na ₂ O	0.01	0.00	0.03	0.00	0.00	0.01	0.02	0.00	0.03	0.03	0.04	0.01	0.02
K ₂ O	0.00	0.00	0.00	0.00	0.00	0.02	0.00	0.00	0.00	0.00	0.00	0.01	0.00
F	0.06	0.06	0.12	0.00	0.19	0.33	0.58	1.28	0.55	0.00	0.03	0.25	n.a.
Cl	0.23	0.32	0.02	0.04	0.04	0.00	0.16	0.10	0.00	0.02	0.00	0.03	n.a.
Total	93.10	93.46	96.05	95.58	95.96	99.18	95.78	95.36	94.38	92.40	95.84	95.70	

Structural formulae on the basis of 50 cations and 78 (O,OH,F,Cl)**

Si <i>apfu</i>	16.24	16.16	17.56	17.24	17.75	17.61	17.79	17.15	17.77	16.56	18.08	17.05	16.12
Al	10.85	11.54	8.96	9.69	9.00	9.41	8.10	10.63	7.79	11.68	9.53	9.56	11.14
Ti	0.01	0.01	0.26	0.02	0.01	0.06	0.68	0.00	0.07	0.00	0.02	0.02	0.00
Fe ²⁺	0.24	0.21	1.97	0.37	0.75	1.50	1.43	0.60	1.30	0.21	1.18	0.79	0.29
Mg	3.12	2.61	2.31	3.36	3.09	2.12	3.35	2.92	3.86	1.96	2.23	2.89	4.51
Mn	0.02	0.00	0.00	0.02	0.00	0.06	0.03	0.00	0.07	0.02	0.04	0.00	0.05
Ca	19.50	19.46	18.92	19.26	19.41	19.21	18.60	18.69	19.11	19.54	18.91	19.67	17.86
Na	0.01	0.00	0.03	0.00	0.00	0.01	0.02	0.00	0.03	0.03	0.04	0.01	0.02
K	0.00	0.00	0.00	0.00	0.00	0.01	0.00	0.00	0.00	0.00	0.00	0.01	0.00
OH	6.04	5.97	5.49	5.91	5.40	5.26	4.59	3.47	5.42	5.59	4.92	5.76	6.38
F	0.10	0.10	0.19	0.00	0.29	0.49	0.90	1.99	0.86	0.00	0.05	0.38	n.a.
Cl	0.03	0.04	0.02	0.03	0.03	0.00	0.13	0.08	0.00	0.02	0.00	0.02	n.a.

* Results of electron-microprobe analyses. *apfu*: atoms per formula unit. ** Groat *et al.* (1993). Abbreviations: tit. Grt: titaniferous garnet, symp. Symplectitic intergrowth.

to the development of tilleyite veins that penetrate the spurrite zone and may follow for some distance the spurrite – melilite boundary. Garnet in these veinlets has the same range of composition as the spines (Grs₄₂, 0.01 wt% TiO₂; Grs₅₂, 0.7 wt.% TiO₂). In the same sample, a vesuvianite – calcite symplectite also appears at the tip of a garnet veinlet that branches out into a recrystallization veinlet in spurrite; tilleyite – calcite symplectites and interstitial grains of calcite occur nearest the spurrite. In wollastonite-dominant exoskarms (CH7, CH1), a narrow rim of the same pale yellow garnet (Grs_{54–72}, 2.38–1.43 wt.% TiO₂) is observed between the earlier titanian garnet or the melilite crystals and tilleyite, with apophyses between the tilleyite crystals. It is associated in some cases with vesuvianite. Vesuvianite crystals with an “idiomorphic” zonation occur in contact with calcite, not far from zone B (Table 8, UCV15, core #15/44, rim #15/42), and may partially replace earlier yellow garnet, as shown by the locally high Ti contents (*e.g.*, #15/8, UCV7).

The boundary BV – C, where modified (UCV9), also shows the development of a vesuvianite – garnet asso-

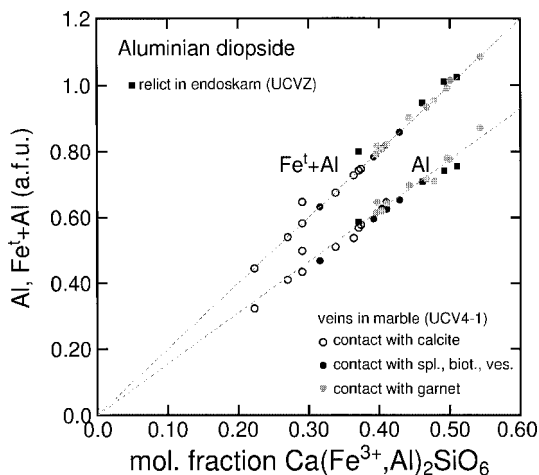


FIG. 11. Compositions of aluminian diopside from endoskarms and skarn veins in the marble at UCV: Al and Al + Fe^{total} (in *apfu*) versus mol. fraction Ca(Al, Fe³⁺)₂SiO₆.

ciation partly at the expense of the melilite crystals already affected by the granular modification. On the wollastonite side, a yellowish garnet (Grs₅₇, 2.0 wt.% TiO₂) forms a rather regular millimetric zone and, in places, a network of anastomosed veinlets enclosing islands of wollastonite; these veinlets may connect this millimetric zone to the rounded crystals of earlier brownish yellow titanian garnet developed at a short distance in the exoskarn. On the melilite side, vesuvianite forms oval patches, changing in turns to colorless grossular (Grs₈₅₋₉₀), including in some places patches of hibschite (Ca₃Al₂Si_{1.7}H_{5.2}O₁₂). In UCV65, the same transformation is widely developed in places where the melilite – wollastonite boundary is not rimmed by titanian garnet, as shown in Figure 2. In CH30, which contains melilite, wollastonite and altered tilleyite, the grossular + vesuvianite association is developed, partly at least, at the expense of wollastonite.

In CH49, large roundish patches of vesuvianite are observed in direct contact with fresh melilite, which shows over a distance of 15 μm a strong but progressive compositional change toward the gehlenite end-member (up to Gh₈₂). The associated garnet is Grs₅₃ with 1.27 wt.% TiO₂. The composition of vesuvianite shows small variations with respect to that given in Table 8 (#4/15).

In some of these occurrences, vesuvianite seems to have been overgrown by (and sealed in) the later yellowish garnet.

Recrystallizations and vesuvianite in endoskarms A

Coarsely recrystallized areas tend to develop as bands parallel to the boundary with the intrusive rock. They contain remarkable instances of successive growth-zones in the garnet and, in some cases, calcite patches and even quartz, which are absent in the finer-grained parts. This recrystallization produces large idiomorphic crystals of grossular, which tend to segregate as irregular veinlets surrounded by large crystals of wollastonite. Xenotite is observed occurring side by side with wollastonite (CH 78). A few small prisms of apatite, included in the garnet, show an incipient substitution of P by Si and S. Hydroxyllellestadite fills most of the interstitial spaces between the idiomorphic crystals of garnet. Other interstitial spaces in the same areas are filled with clinocllore or “pennine”, or a mixture of “pennine” and chrysotile. Chrysotile was also observed in the same situation associated with minor calcite and rare anhydrite.

Fine-grained subidiomorphic vesuvianite appears as large patches, which may predominate (UCVZ) but, more commonly, constitutes only a fraction of the rock (CH4, CH8, UCV60, UCV61); it tends to form discontinuous veinlets roughly parallel to the contact with the intrusive rock. Such veinlets locally replace titanian garnet (UCV 60 and 61). The associated minerals are grossular, chlorite, chrysotile, calcite and scarce pure diopside, in large idiomorphic crystals. In CH6, a cross-

TABLE 9. MINERAL-FLUID REACTIONS RELEVANT TO THE SKARNS OF CORNET HILL AND UPPER CERBOAIA VALLEY, ROMANIA, REPRESENTED IN EQUILIBRIUM DIAGRAMS

Til = Spu + CO ₂	(1)	[CaTs] + Cal = [Gh] + CO ₂	(24)
2 Wo + 3 Cal = Til + CO ₂	(2)	[Di] + Cal = [Ak] + CO ₂	(25)
4 Wo + Spu = 3 Rnk + CO ₂	(3)	2 [An] + 2 Cal = [Grs] + [CaTs] + 2 CO ₂	(26)
[Grs] + Cal = [Gh] + 2 Wo + CO ₂	(4)	3 [Grs] + 2 Spl + 5 Cal = 5 [Gh] + 2 [Ak] + 5 CO ₂	(27)
[Grs] + 4 Cal = [Gh] + Til + 2 CO ₂	(5)	2 [Di] + 5 [CaTs] + 2 Cal = 3 [Grs] + 2 Spl + 2 CO ₂	(28)
[Grs] + 4 Cal = [Gh] + Spu + 3 CO ₂	(6)	Cal + SiO ₂ = Wo + CO ₂	(29)
3 [Grs] + Til = 3 [Gh] + 8 Wo + 2 CO ₂	(7)	Til + 3 SiO ₂ = 5 Wo + 2 CO ₂	(30)
3 [Grs] + Spu = 3 [Gh] + 8 Wo + CO ₂	(8)	5 Cal + 2 SiO ₂ = Til + 3 CO ₂	(31)
[Grs] + Spu = [Gh] + 2 Rnk + CO ₂	(9)	Spu + 3 SiO ₂ = 5 Wo + CO ₂	(32)
[Grs] + Rnk = [Gh] + 4 Wo	(10)	5 Cal + 2 SiO ₂ = Spu + 4 CO ₂	(33)
Rnk + 8 Ves = 35 [Grs] + 9 [Gh] + 16 [Ak] + 36 H ₂ O	(11)	Rnk + SiO ₂ = 3 Wo	(34)
Wo + 2 Ves = 9 [Grs] + 2 [Gh] + 4 [Ak] + 9 H ₂ O	(12)	3 Spu + 4 SiO ₂ = 5 Rnk + 3 CO ₂	(35)
Spu + 16 Ves = 69 [Grs] + 19 [Gh] + 32 [Ak] + CO ₂ + 72 H ₂ O	(13)	[Gh] + SiO ₂ = [CaTs] + Wo	(36)
Til + 16 Ves = 69 [Grs] + 19 [Gh] + 32 [Ak] + 2 CO ₂ + 72 H ₂ O	(14)	[Ak] + SiO ₂ = [Di] + Wo	(37)
Cal + 4 Ves = 17 [Grs] + 5 [Gh] + 8 [Ak] + CO ₂ + 18 H ₂ O	(15)	[Gh] + Wo + SiO ₂ = [Grs]	(38)
69 Cal + 4 Ves = 22 [Gh] + 8 [Ak] + 17 Til + 35 CO ₂ + 18 H ₂ O	(16)	[Gh] + 1/3 Rnk + 4/3 SiO ₂ = [Grs]	(39)
69 Cal + 4 Ves = 22 [Gh] + 8 [Ak] + 17 Spu + 52 CO ₂ + 18 H ₂ O	(17)	[Gh] + 1/5 Spu + 8/5 SiO ₂ = [Grs] + 1/5 CO ₂	(40)
3 Til + 2 Ves = 11 [Gh] + 4 [Ak] + 23 Wo + 6 CO ₂ + 9 H ₂ O	(18)	2 Ves + 6 SiO ₂ = 11 [Grs] + 4 [Di] + Wo + 9 H ₂ O	(41)
3 Spu + 2 Ves = 11 [Gh] + 4 [Ak] + 23 Wo + 5 CO ₂ + 9 H ₂ O	(19)	11 [Gh] + 4 [Ak] + 8 Wo + 9 SiO ₂ + 9 H ₂ O = 2 Ves	(42)
9 Rnk + 2 Ves = 11 [Gh] + 4 [Ak] + 35 Wo + 9 H ₂ O	(20)	11 [Gh] + 4 [Ak] + 8 Cal + 17 SiO ₂ + 9 H ₂ O = 2 Ves + 8 CO ₂	(43)
[Ak] + 2 Mtc + Spu = 3 Mer + CO ₂	(21)	Spl + 4 Cal + 3 SiO ₂ = [Gh] + [Ak] + 4 CO ₂	(44)
17 Spl + 44 Cal + 6 Ves = 50 [Gh] + 29 [Ak] + 44 CO ₂ + 27 H ₂ O	(22)	Mtc + Cal + SiO ₂ = [Ak] + CO ₂	(45)
[Gh] + [Di] = [Ak] + [CaTs]	(23)	2 [Ess] + [Grs] = 2 [CaTs] + [And]	(46)

Square brackets indicate end-member in a solid-solution series. Symbols: Ak: åkermanite, An: anorthite, Cal: calcite, CaTs: calcium Tschermaks component of clinopyroxene, CaAl₂SiO₆, Crn: corundum, Di: diopside, Ess: esseneite, Gh: gehlenite, Grs: grossular, Mer: Merwinite, Mtc: monticellite, Rnk: rankinite, Spl: spinel, Spu: spurrite, Til: tilleyite, Ves: vesuvianite, Wo: wollastonite.

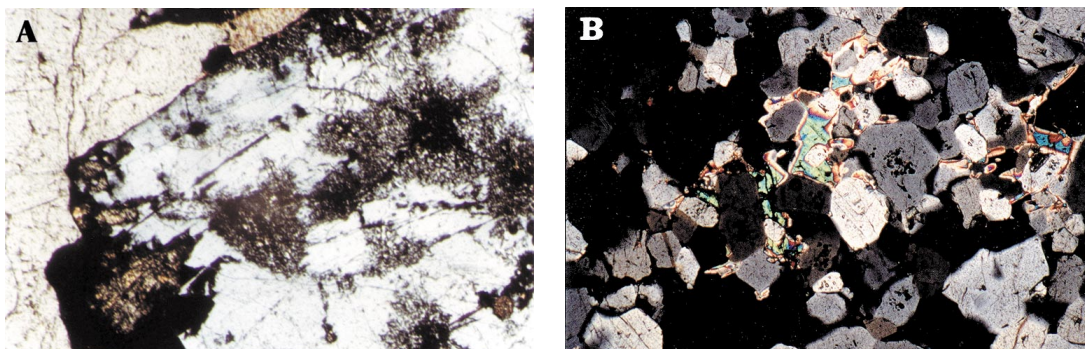


FIG. 12. Photomicrographs of the secondary modifications of the melilite veins. A. Along the boundary between a large idiomorphic crystal of melilite (partly altered in the lower left part) and a very large prism of wollastonite (exoskarn), calcite replaces wollastonite, and patches of granular modification (gehlenite – monticellite – grossular) appear in melilite. Width of field is 2.6 mm. Cross-polarized light. B. Veinlets of monticellite (brightly colored) interstitial between melilite crystals that include grains of garnet. Width of field is 2.6 mm. Cross-polarized light.

cutting vein of diopside, 0.5 mm thick, is surrounded on both sides by a millimeter-wide zone entirely devoid of pyroxene, containing some vesuvianite in addition to recrystallized grossular.

The alteration of melilite

In a few samples, melilite is altered along veins to yellow garnet (Gr_{S25–30}, 4.07–5.60 wt.% TiO₂), with clusters of perovskite (CH3, CH49). The development of this garnet starts on earlier-formed grains of titanian yellow interstitial garnet of zone BV. A more-or-less gradual zonation can be observed from the yellow garnet to pale yellow (*e.g.*, Gr_{S47}, 2.93 wt.% TiO₂) and finally colorless garnet (Gr_{S51–67}, 2.51–1.27 wt.% TiO₂; *e.g.*, #4/8, Table 5) in contact with vesuvianite.

Melilite also may be altered to vesuvianite, a bicchulite-like mineral and a kamaishilite-like mineral; small patches of vesuvianite (without calcite) develop on melilite (*e.g.*, CH49, #8/17, Table 8). Near such vesuvianite and even at its contact, the optical continuity of the melilite crystal is preserved (no difference in either orientation, birefringence or indices of refraction), but the crystal becomes isotropic, with a sharp boundary with melilite. The electron-microprobe analyses of this isotropic region and its immediate vicinity (Table 6, #8/18) suggest that the cubic mineral is bicchulite, considered by Henmi *et al.* (1973) as a hydrated melilite-group mineral, and the anisotropic surrounding region is kamaishilite, which has been interpreted as a tetragonal polymorph of bicchulite (Uchida & Iiyama 1981), although the compositions are in fact different.

Alterations of melilite in zone BV also include “bicchulite” occurring as a later alteration along a distinct network of veins. Where this alteration becomes extensive, it is accompanied by the development of vesuvianite as cores in the same veins. Similar vesuvian-

ite replaces melilite in part of the melilite veinlets in exoskarns (#37/49, Table 8), the replacement of idiomorphic crystals leads to a peculiar aspect and a composition richer in Al than usual. Locally, this vesuvianite recrystallizes into large zoned patches with the usual aspect and composition. In UCV9 and UCV65, large polycrystalline patches of vesuvianite occur at a few places as pseudomorphs after melilite, side by side with the predominant granular patches. Neither of them was observed to enclose or be modified by the other. On the other hand, vesuvianite has been mentioned to replace the center of some granular patches.

In zone B, large monocrystalline patches of vesuvianite are associated with altered zones in which wollastonite is more-or-less preserved, but melilite is always completely altered (CH3 and CH57). The birefringence and composition of this vesuvianite (Table 8, #2/10 and 2/12) are variable; it has low contents of Ti, F and Cl compared to that described above, but may show a complex zonation, with a slight decrease in Al and increase in Fe contents toward the rim.

The alteration of melilite also may lead to a cebollite-like mineral. This product is perhaps the most commonly observed type of alteration of melilite, and consists of brownish aggregates of fine fibers, the composition of which resembles that of cebollite, *e.g.*, Mg_{0.53}Ca_{4.04}Al_{2.08}Si_{2.96}O₁₂(OH)_{3.24}.

Other alteration assemblages

Other alteration assemblages are mostly restricted to wollastonite in veins and remain local. Patches of a mineral of foshagite-like composition are observed as a product of the incomplete replacement (with clear boundary) of the large crystals of wollastonite in the veins. A mineral of mountainite composition occurs as rare small grains in the same veins. A Cl-bearing vari-

ety is also observed as a late product in the heavily altered parts of CH3. Mountainite is a CSH mineral with a Ca:Si ratio lower than foshagite, wollastonite and xonotlite, but containing potassium (in this case, 0.7 wt.% K₂O). Cl-free djerfisherite, also a K-bearing mineral, exceptionally occurs as a secondary modification of pyrrhotite in CH51.

INTERPRETATIONS

One of the problems raised by the high-temperature skarns at Apuseni is the origin of the massive melilite-dominant rocks. Together with the occurrence of tilleyite, spurrite, monticellite and hydroxyllestadite, their presence is the most spectacular feature of these skarns. Similar associations of minerals have been observed in the monticellite zone of the skarns at Crestmore, California (Burnham 1959), where they were interpreted to have developed at the expense of the Mg-bearing marble. However, there is no Mg-bearing marble in the vicinity of CH and UCV, and melilite at Crestmore never forms monomineralic bodies as in the Apuseni Mountains, although its composition (Gh₆₀) is, with a few exceptions, in the same range in both occurrences.

The texture of wollastonite in endoskarms

The parallel-fiber texture of wollastonite (zones A and B) can be understood as resulting from its growth at a metasomatic front as defined by Korzhinskii (1970), *i.e.*, from the fact that the fluid–rock disequilibrium, therefore chemical reaction, was restricted in space to the surface that separated the wollastonite zone from the adjacent one.

The usual acicular shape of wollastonite crystals indicates that the growth kinetics of the (*h0l*) faces are much slower than the others under conditions of high disequilibrium. Therefore, the wollastonite crystals that had their *c* axis perpendicular to the front grew faster than the others, which thus remained within the wollastonite zone, at the rear of the front where the fluid–rock interaction took place, and ceased to grow. A state of parallel growth was quickly reached, and persisted as long as the growth process went on.

The rock at the immediate contact of zone A, where observed, is always a (quartz-free) “syenite”; in this case, the mineral that was transformed into wollastonite was not quartz but alkali feldspar, and grossular was formed simultaneously. In a case of limited mobilization of Al and Si, the resulting rock has a uniform proportion of grossular and wollastonite in parallel prisms, which is as a first approximation what is observed in zone A.

There are two discordant observations (CH8 and CH22) in the outer part of zone A3, close to the exoskarn boundary: a fan-like organization of wollastonite contrasts with its tendency to constitute monomineralic

patches (Fig. 4D). The same textural relation has been noticed between wollastonite and melilite in zone B (Fig. 7B), with circular arrays of wollastonite prisms, the centers of which are occupied by one or a few large crystals of wollastonite. In agreement with the assumed mode of development of wollastonite, we believe that the arrays are reaction rims around quartz grains. As a result, (1) the melilite – wollastonite association of zone B derives from the grossular – wollastonite association of zone A, and the whole region that displays the fibrous texture of wollastonite, zones A and B, is an endoskarn, formed by the infiltration into the pre-existing intrusive rock (on the scale of a few centimeters) of Ca-rich fluids circulating in the region of the contact. The boundary between the zones B and C thus corresponds to the former boundary of the intrusive rock, in accordance with the striking difference in grain size and texture of the wollastonite crystals between these zones. (2) The endoskarn at the inner limit of the exoskarn was not developed at the expense of the quartz-free “syenite” but at the expense of the quartz-bearing monzodiorite. The presence, in two samples, of a few large rectangular ghosts of zoned plagioclase (which do not exist in the syenite) is consistent with this interpretation. This conclusion is also supported by the fact that melilite, which is by far the predominant Al- and Mg-bearing mineral in the entire zone B, has the same Al:Mg ratio as the monzodiorite, not the “syenite” (Fig. 13, analyses in Piret 1997). The “syenite”, which has been shown to have pegmatitic–hydrothermal features, most probably developed as a late evolution of the intrusive rock. The portion of zone A that shows the parallel wollastonite texture formed at its expense.

The “melilite vein” stage and its subsequent evolution

The melilite ± wollastonite zones, observed on both sides of the former intrusive contact, show occasional variations in the sequence of zones (the absence of melilite in CH22 and the spurrite – melilite association of CH49 are the most conspicuous examples). Another irregular feature is the proportion of the fibrous-wollastonite-bearing endoskarn that belongs to zone B; it is practically absent in CH8 and well developed in other samples from CH. *As a consequence, the development of melilite ± wollastonite cannot be interpreted as belonging, together with other endoskarms, to a single synchronous metasomatic sequence. Melilite development was secondary after, and discordant on, pre-existing skarns.* These early skarns, which cannot be precisely defined by observation owing to their reworking, are tentatively characterized below.

The melilite ± wollastonite association of the vein stage

At CH, the massive melilite vein that developed along the endoskarn – exoskarn boundary contains no

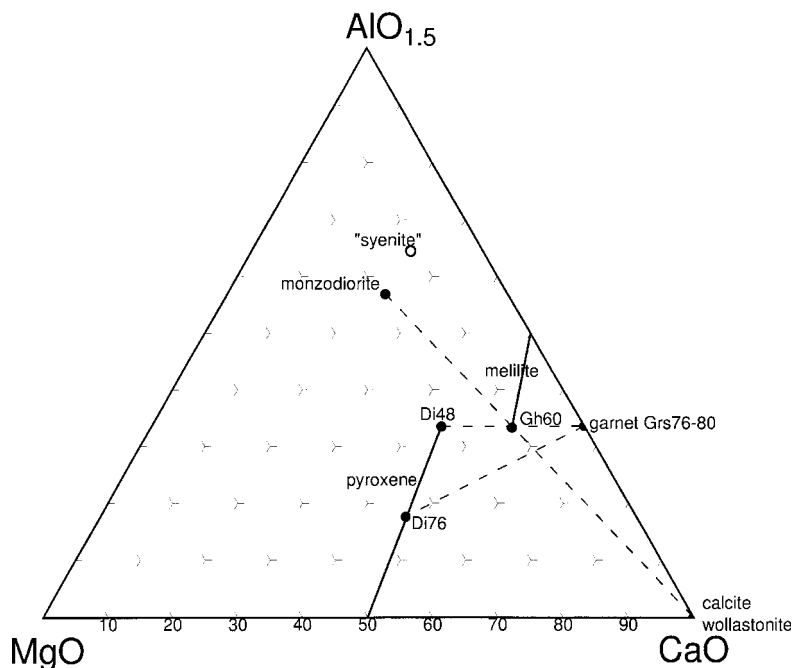


FIG. 13. Projection of the compositions of monzodiorite, "syenite" and skarn minerals on the $\text{CaO}-\text{AlO}_{1.5}-\text{MgO}$ plane (mol. fractions).

wollastonite, except along its outer side, where the proportion of medium-grained crystals of wollastonite increases sharply, up to the rather blurred contact with the exoskarn, formerly composed of wollastonite and probably calcite (and later of wollastonite and tilleyite). However, the vein is not in every case strictly located at the contact with zone B. In places, it is separated from zone B by 1–2 mm of massive wollastonite with similar medium grain-size and texture as the exoskarn bordering the vein; the change of grain size and texture at the limit of zone B is very sharp (Fig. 9A).

At UCV, a different type of crystallization (or recrystallization) of the melilite results in a completely idiomorphic shape of the melilite crystals, which commonly are very coarse-grained and show extreme changes of dimensions everywhere. Melilite largely predominates over the associated minerals up to the sharp contact with the wollastonite – calcite exoskarn, where only rare veinlets of coarse melilite are observed. The extreme variability of grain size is typical of pegmatites, and the porphyroblastic tendency of the melilite in the adjacent part of zone B is reminiscent of a vein influence. The relation of zone BV with zone B is, as a first approximation, the same as at CH, except for the absence of the outer part of endoskarns (characterized by the wollastonite arrays). It is the case with sample

UCV8, which shows a large development of "zone" BV at the expense of endoskarns.

The simplest way to understand the relation between the veins and zone B is to assume that the endoskarn B developed under the influence of the vein-forming fluid, by transformation of a wider or narrower part of endoskarn zone A (diopside – grossular – wollastonite) to fine-grained melilite Gh_{60} + wollastonite, with a more-or-less preserved texture.

Another analogy between the veins BV at CH and UCV is that many samples of the UCV suite show a striking tendency for the proportion of wollastonite to decrease owing to its replacement by melilite. This replacement, as well as the development of melilite veins along the exoskarn boundary and within the exoskarn at CH, involve the addition of Al and Mg. An obvious source for Mg is zone A2, from which pyroxene disappeared through its transformation into A3. Clearly, Mg was mobile in the vein-forming process, and even perfectly mobile in the vein itself, as shown by the fact that the melilite in the vein has exactly the same composition as the melilite in zone B (the sole exception occurring in sample CH49), in spite of contrasted modes of development and association.

Directly related to this zone of recrystallization is the incidence of titanian garnet, which replaced wollas-

tonite (zones B and C) and started to develop in zone C practically at the same time as melilite, as it includes small idiomorphic crystals of melilite and occurs side by side with coarser-grained melilite. The crystallization of titanian garnet in a rock originally composed of pure calcite implies that *titanium also was displaced by the fluids*, circulating on both sides of the B–C boundary. Perovskite, which appeared prior to titanian garnet and occurs commonly in endoskarms near the contact with the “syenite” (and, in one case, the exoskarn), is absent from the largest part of endoskarms. In most cases, it disappeared not by replacement by other Ti minerals (exceptions are locally observed in CH49, CH7, UCV61 and possibly CH3), but by leaching out of titanium, which was redeposited as titanian garnet during the vein stage.

Tilleyite appeared at CH in equilibrium with melilite and before the titanian garnet, as shown by the observation of tilleyite inclusions in titanian garnet that developed in equilibrium with melilite. It developed extensively at the expense of calcite and some parts of the pre-existing spurrite and wollastonite, forming a zone a few dm thick, at least, in contact with the marble and penetrating along veins in the inner zones. Tilleyite remained stable in association with vesuvianite before ultimately being altered, in many samples, to wollastonite + calcite.

The high-temperature granular modification (monticellite stage) and the crystallization of titanian garnet

The usual pattern of occurrence of monticellite is the granular modification, which immediately postdated the vein stage and has exactly the same areal extent. It is characterized by the development of a three-phase association (gehlenite, monticellite and a Si–Ca mineral, which seems to have been originally rankinite). Compared to the earlier melilite – wollastonite stage, the addition of one mineral indicates that one of the characteristic features of this modification is the increase in the number of inert components. The appearance of garnet in the granular patches can be interpreted in a similar way, by a further increase of the number of inert components.

The change of a component from a perfectly mobile to an inert status in an abstract notion. In concrete terms, “perfectly mobile” means that the chemical potential of this component is ruled by the fluid, which implies long-continued flow of a fluid of constant composition, usually resulting in a decrease in the number of associated phases at equilibrium. An increase in the number of phases, limited to a local scale, as observed in the case of the granular modification, may be expected to result from a reduced flow of fluid associated with a change in physical or chemical conditions, such as a drop in temperature or the infiltration of a different fluid in small amount, with modifications controlled by the access of

this fluid. Therefore, we believe that from this stage on, the large-scale metasomatic activity of the vein stage is over.

Although titanian garnet appeared during the main melilite – wollastonite stage, its largest development generally followed the granular modification. In such cases, it was probably in equilibrium with the minerals that constitute the granular patches, as suggested by its development around the patches, as a replacement of wollastonite. It first developed in a typical sporadic porphyroblastic manner, which indicates a difficulty in nucleation; in most cases, the growth started at the expense of wollastonite. Its zonation, never oscillatory, shows that its Ti content was highest at first (and highly variable at a given place, in the range 11–4 wt.% TiO₂, with a remarkable correlation with the Mg contents, which reach 0.89 wt.% MgO), and decreased in subsequent stages of growth. This may distinguish it from the titanian garnet formed in other skarns related to the low-temperature, mineralization-bearing andradite stage. As for Mg, an obvious source for Ti is the endoskarn zone A, from which this element was leached; but in contrast with Mg, Ti cannot enter the melilite structure, so that its precipitation required nucleation of garnet, under probable conditions of oversaturation. Owing to an overstepping of the reaction, the growth of garnet was probably very rapid at first, then slower, more irregular, using preferentially the intergranular spaces between other minerals, but without further nucleation (hence the “spine” texture). Its regular compositional change is consistent with the assumed initial oversaturation of Ti in the fluid, and also with a decrease in the rate of fluid flow.

The granular modification occurred in relation with fracturing, exceptionally clear in CH51, just as the tilleyite – vesuvianite stage in CH49. The somewhat discontinuous character of these stages is consistent with the idea that these transformations depended on the local availability of fluids along very discrete microfractures.

The mode of occurrence of vesuvianite

When compared to other skarns in which it plays an essential role, vesuvianite is striking at CH and UCV by its late, irregular and sporadic mode of occurrence. It forms a secondary zone developed by reaction between zones A and B, as suggested by the relation observed in UCVZ. Together with grossular, it forms another secondary zone between the melilite crystals, already affected by the granular modification, and the wollastonite in zone C. In this case, vesuvianite alternates with the pale yellow garnet developed later than the grossular. Garnet – calcite – vesuvianite veins, associated with the tilleyite veins (CH49), were interpreted as the product of the local transformation of melilite + spurrite. Vesuvianite also is a product of secondary transformations in regions with Mg-bearing minerals, without relation to the zonation, for example as a pseudomorph after

melilite in the exoskarns and patches in the endoskarns. It may be one of the alteration products of melilite, post-dating the granular modification. Finally, it may evolve from the “kamaishilite” – “bicchulite” type of alteration, of which it constitutes the third product.

Vesuvianite occurrence is thus invariably secondary, and restricted to places where Mg was locally available, suggesting that its irregular distribution is due to its late formation, at a stage at which Mg was no longer mobile.

The spurrite – perovskite – melilite association of the first-stage endoskarns

The occurrence of perovskite pseudomorphs after titanite in the inner part of zone A1 and in one exoskarn sample indicates that Si was leached out while Ti had a perfectly inert behavior, prior to the vein stage. The most striking example of a preserved original distribution of the Ti minerals among CH and UCV skarns is provided by the banded sample CH49, which is also the only perovskite-rich rock of our collection. The development of spurrite + melilite in this sample, instead of the more usual wollastonite + melilite association, accounts for a stronger undersaturation in silica. In another spurrite-bearing sample (CH1), spurrite is observed as relics with respect to tilleyite. Even in CH49, there are many indications that the spurrite – melilite association is a relict one; on the outer side, the reworking of the spurrite into tilleyite ± calcite, and on the inner side, the modification of melilite to gehlenite at the contact with grains of vesuvianite, are indications of the role of the later fluids responsible for the high-temperature modifications.

Taking into account also the exceptional narrowness of the zone system in this sample (2 cm) and the mosaic, metamorphic-like texture of the inner part of the sample, it is probable that only a small amount of fluid was involved in the (re)crystallization of the observed association. The difference in composition of melilite between this sample and all others, mentioned above, may be more than merely accidental, and may indicate that its Mg:Al ratio was not affected by the uniformization in melilite composition so conspicuous elsewhere. We suggest that this rock was little affected by the major influx of fluid characterized by Ti and Mg mobility, and that its strong undersaturation in silica was reached in the early, Ti- and Mg-inert stage.

The grossular – aluminian diopside association of the first-stage endoskarns

The absence of any Mg-bearing mineral in zone A3 has been interpreted as an indication of reworking of this zone at the vein stage. Some indications of the earlier association of minerals were found in sample UCVZ; it contains inclusions of grossular and aluminian diopside very different in both composition and texture from those of the intrusive rocks and zone A2. The only

other observed occurrence of the same association is the vein network in marble (UCV4–1), with striking similarities in the compositions of minerals (Fig. 11). Therefore, we suggest that they have the same origin. As, in the case of sample UCVZ, the original material is the intrusive rock, the veins in sample UCV4–1 may have been derived from magmatic veins in the marble (the perovskite aggregate replacing titanite, observed in exoskarn sample CH7, also suggests the former presence of an apophysis of the intrusive body in the surrounding exoskarn).

Owing to the immediate proximity of a melilite crystal (also relict in a wollastonite vein), the grossular – aluminian diopside association in sample UCVZ is interpreted as the former zone A of the endoskarn, at the expense of which zone B developed. In addition, the crystals of aluminian diopside in sample UCVZ and some of those in UCV4–1 have high Ti contents, indicating that Ti was not leached out of these rocks when the pyroxene crystallized. This association is thus interpreted as characteristic of the outer part of the early endoskarn, considered as the first stage.

Early fractures in the first-stage endoskarns

Another possible confirmation of the early development of these associations is found in the fact that samples UCV4–1 and CH49 are the only ones that show evidence of fracturing, and shearing of the endoskarn – exoskarn boundary in the case of CH49. Such a strong deformation was not observed in the wollastonite crystals of CH or UCV, except to a moderate extent in CH30, although deformation of wollastonite is commonly observed in skarns in general. Our tentative conclusion is that *most of the wollastonite – melilite skarns developed after this episode of deformation*. The irregular nature and discordant character of the melilite “zone” in many samples, stressed above as a strongly distinctive feature of the modes of occurrence of melilite, are perhaps due to the existence of pathways for later fluids, opened at the time of fracturing.

PHYSICO-CHEMICAL CONSTRAINTS FROM THERMOCHEMICAL MODELING

Thermochemical calculations

The conditions of stability of the mineral associations described have been calculated as function of temperature, pressure of CO₂ and activity of aqueous silica (Figs. 14–18, Table 9). The THERMOCALC database and software (Holland & Powell 1998) were chosen for most calculations, as they include data for spurrite, tilleyite and vesuvianite. We assumed that the garnet on the join grossular–andradite and melilite on the join gehlenite–åkermanite are ideal, respectively two-site and one-site solid solutions (Perchuk & Aranovich 1979, Charlu *et al.* 1981). Although no model for vesu-

vianite solid-solution is available, the vesuvianite composition available in the THERMOCALC database [$\text{Ca}_{19}\text{Mg}_2\text{Al}_{11}\text{Si}_{18}\text{O}_{69}(\text{OH})_9$] was considered close enough to the measured ones to be used. Monticellite could not be considered; according to the database, monticellite should not be stable in association with either gehlenite-rich melilite or rankinite, contrary to our observations.

As the compositions of pyroxene encountered have a comparatively high content of the esseneite end-member, for which no thermochemical data are available in the THERMOCALC database, the set of equilibria involving this mineral (Fig. 18) was calculated from Sack & Ghiorso (1994a, b) for the thermodynamic properties of pyroxene, melilite and plagioclase, and from Berman (1988) for other minerals, as recommended by Sack & Ghiorso (1994b). In all calculations, the CaTs and esseneite mole fractions in aluminian diopside are taken to be equal, in accordance with the analytical data (Fig. 11).

With the exception of monticellite, the calculated equilibria were found to be consistent with the observed associations and compositions of minerals. The consistency between calculations from THERMOCALC and Berman + Sack databases was checked for the equilibrium (4) $[\text{Gh}] - \text{Wo} - \text{Cal} - [\text{Grs}] - \text{CO}_2$; the fugacity of CO_2 was calculated to be 50 bars (750°C) in the former case and 68 bars in the latter. We did not correct for this discrepancy.

The activities and molalities of aqueous silica, taken to be equal, have been determined from the solubility of quartz in H_2O (Manning 1993).

The pressure of H_2O

The only OH-bearing mineral found in the high-temperature associations of skarn minerals is vesuvianite

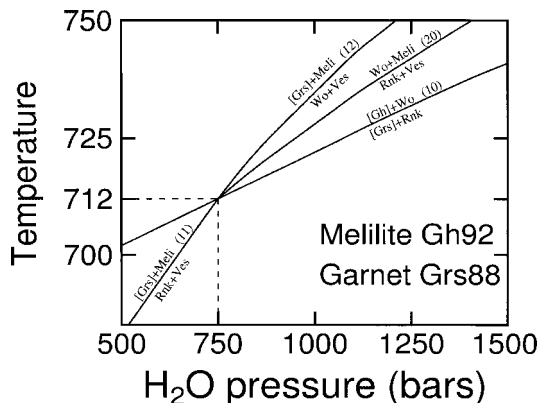


FIG. 14. $P(\text{H}_2\text{O}) - T$ relationships between melilite (Gh_{92}), garnet (Grs_{88}), vesuvianite, wollastonite and rankinite. Abbreviations and reaction stoichiometries in Table 9.

(except for xonotlite, for which no thermodynamic data are available). It developed in the granular patches of melilite after the association of melilite Gh_{92} with the mineral of rankinite composition and garnet Grs_{88} (UCV9), in apparent equilibrium with wollastonite. In the system $\text{SiO}_2 - \text{Al}_2\text{O}_3 - \text{CaO} - \text{MgO} - \text{H}_2\text{O}$ (Fig. 14), the invariant point vesuvianite – melilite (Gh_{92}) – garnet (Grs_{88}) – wollastonite – rankinite is located at 712°C and 750 bars H_2O pressure; at lower H_2O pressure, vesuvianite (eq. 11, Table 9) appears at a lower temperature than rankinite (eq. 10), in accordance with the observation. Therefore, H_2O pressure was lower than 750 bars, in agreement with the approximate value of 500 bars estimated for the magmatic stage. The stability conditions of the mineral associations have been calculated at 750 bars, which may lead to an overestimation of temperatures for the vesuvianite-bearing associations, but this choice has no appreciable bearing on the temperature ranges of associations of OH-free minerals.

The vein stage (melilite)

The association melilite – wollastonite is unstable below a temperature that has a small dependence on CO_2 pressure: 722°C (low pressure of CO_2) to 741°C (wollastonite – calcite equilibrium) (Fig. 15). The composition of garnet in equilibrium with melilite gives further constraints on temperature. As it depends not only on temperature, but also on the activity of silica, as shown by equilibria (38) to (40) in Table 9, the values corresponding to various associations of minerals have been calculated (Fig. 16). The composition chosen for Figure 15 (Grs_{76}) is that of the earliest garnet found in apparent equilibrium with melilite and wollastonite at UCV. It indicates 741°C as the lowest temperature for the melilite-bearing skarns [curve (12), square in Fig. 16]. In the hydroxyllellstadite-bearing sample CH51, the primary garnet is Grs_{59} . As hydroxyllellstadite occurs associated with melilite in CH49, with a composition similar to that of CH51, between spurrite – melilite and wollastonite – melilite “zones”, we assume that this mineral is stable at an activity of silica close to that of the wollastonite – spurrite equilibrium. For a pressure of CO_2 of 11 bars, determined to be the lowest one consistent with the garnet (Grs_{59}) – melilite – wollastonite – spurrite equilibrium, the corresponding temperature is 754°C [dot on curve (8), Fig. 16]. A temperature of 750°C is thus considered to provide a realistic representation of the vein stage.

All the mineral associations described in zones B, C and D imply a low pressure of CO_2 . The sequence W of UCV corresponds to a CO_2 pressure between 22 bars at 750°C (direct contact between calcite and wollastonite, without spurrite or tilleyite) and 26 bars (garnet Grs_{76} in equilibrium with melilite and wollastonite).

For the sequence S at Cornet Hill, the stability of spurrite implies a maximum CO_2 pressure of 16 bars,

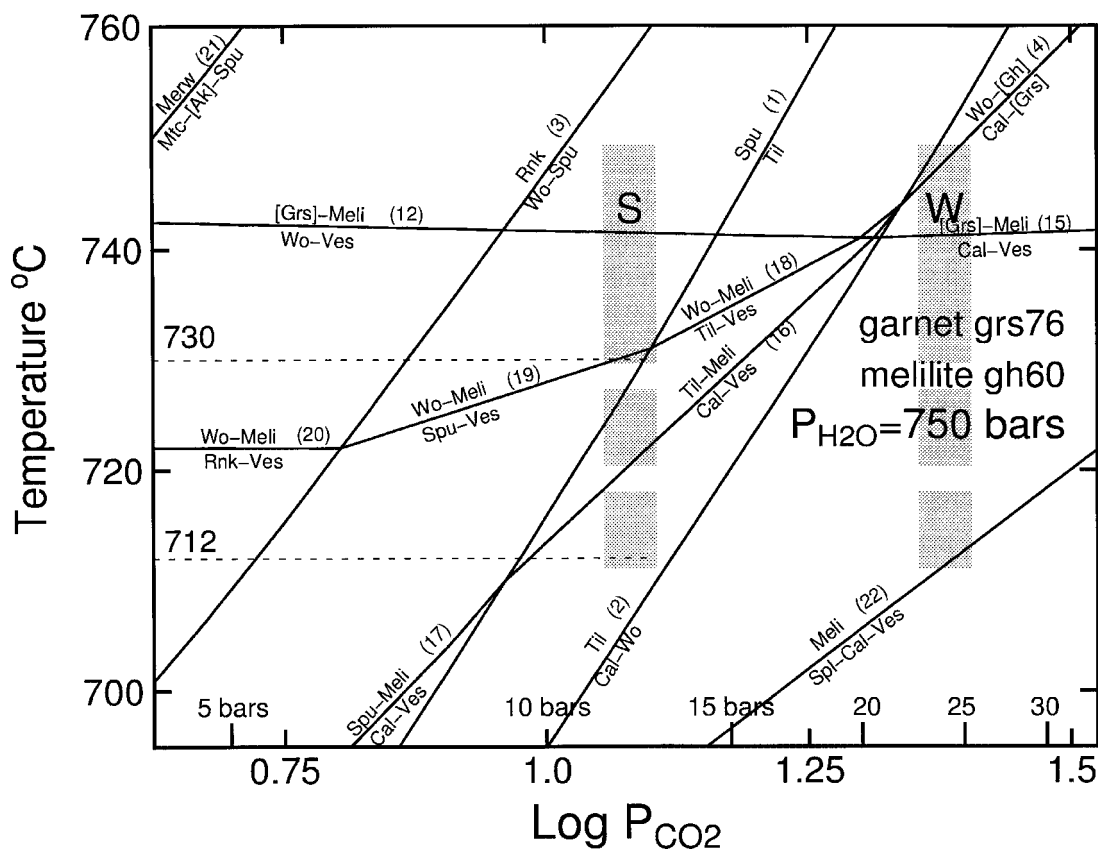


Fig. 15. Low $P(\text{CO}_2)$ portion of the $T - P(\text{CO}_2)$ diagram calculated in the system $\text{SiO}_2\text{-CaO-Al}_2\text{O}_3\text{-MgO-H}_2\text{O-CO}_2$. The conditions of the vein stage at CH (S, melilite - wollastonite - spurrite - tilleyite) and UCV (W, melilite - wollastonite - calcite) are indicated by the grey areas, those of the high-temperature modifications, by the dashed areas. Reaction stoichiometries are indicated in Table 9.

whereas a minimum of 11 bars has been inferred from the association in sample CH51. As we have concluded that some of the spurrite-bearing associations preceded the melilite - wollastonite vein stage, the question arises whether the associated fluids were different. Assuming that the pressure of CO_2 remained constant while the temperature decreased after the end of the main stage of fluid flow, the presence of tilleyite still stable at the vesuvianite stage (and generally subsequently altered) would indicate that the pressure of CO_2 was less than 13 bars (Fig. 15), a value consistent with the stability of spurrite at 750°C and with the assumption that spurrite, melilite and tilleyite were formed under similar conditions of CO_2 pressure.

The stability fields of the mineral associations in the skarns have been calculated at 750°C as a function of $\log a(\text{SiO}_2)$ (Fig. 17). The melilite - wollastonite - pyroxene equilibrium, which separates zones B and A, has been calculated for the pyroxene in equilibrium with

melilite Gh₆₀. The calculated composition ($\text{Di}_{76}\text{CaTs}_{12}\text{Ess}_{12}$, *i.e.*, 8.5 wt% Al_2O_3) is in the range found for pyroxene in zone A2 (CH6, CH8). Silica activity is observed to decrease throughout the entire sequences from zone A to calcite. The limit titanite - perovskite, not represented, corresponds to $a(\text{SiO}_2) = 10^{-2.5}$, a value consistent with the position of this front between the pyroxene - wollastonite - garnet endoskarn and the "syenite". In the melilite-bearing zones, increasing activity of silica resulted in increasing grossular content of garnet, from Gr₅₀ in equilibrium with spurrite - calcite, to Gr₆₅ in equilibrium with spurrite - wollastonite, and Gr₈₁ in equilibrium with melilite - pyroxene, in accordance with the observed compositional ranges. The silica concentration of the fluid in the melilite-bearing zones was very low, in the range 2.9 to $14.5 \times 10^{-4} m$, or 7-35 ppm Si.

The development of tilleyite instead of spurrite, in stable association with melilite and commonly wollas-

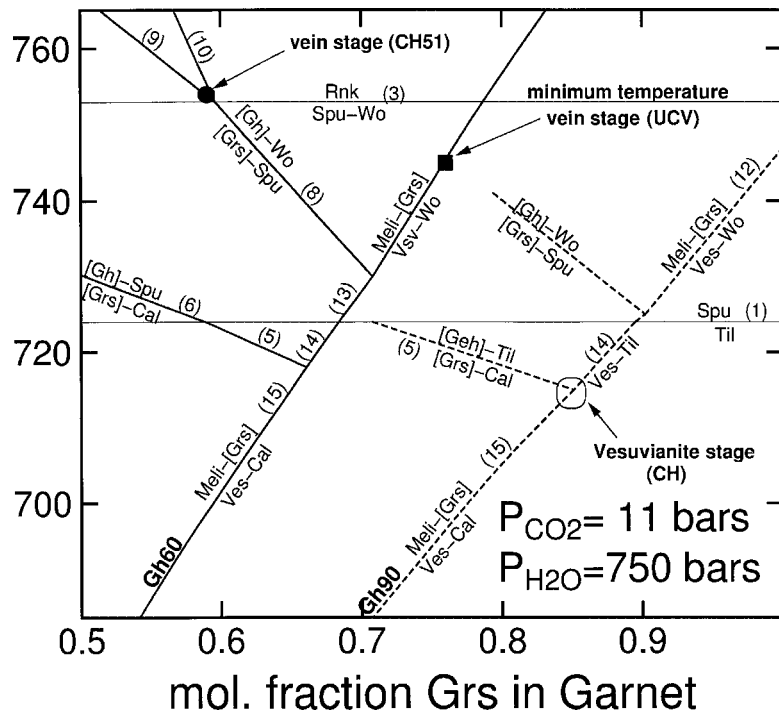


FIG. 16. Garnet composition at equilibrium with melilite, vesuvianite and either wollastonite, rankinite, tilleyite or spurrite, for melilite Gh₆₀ (solid lines) and Gh₉₀ (dashed lines).

tonite, most probably results from a lower temperature (Fig. 15). Tilleyite is stable at 730°C in a range of fluid compositions that corresponds at 750°C to spurrite and to the spurrite – calcite boundary (Fig. 17), in agreement with the largest development of tilleyite on the marble side of the exoskarn. This interpretation is all the more likely as the development of tilleyite in equilibrium with melilite is followed by the tilleyite – vesuvianite association, which is stable only below 730°C. The circulation of the same fluid, mainly along fractures, is probably responsible for the locally observed replacement of wollastonite by tilleyite, indicating leaching of silica in the inner part of the exoskarms.

Secondary modifications

As indicated above, the association constituting the monticellite-bearing granular patches is inferred to be unstable. However, as the progressive destabilization of the åkermanite component of melilite into monticellite + rankinite or OH-bearing Ca–Si minerals is similar to the experimentally observed decomposition of åkermanite into monticellite + wollastonite below 700°C (Harker & Tuttle 1956), it probably occurred under decreasing temperature.

The association of vesuvianite with grossular (Gr_{S85-90}) and gehlenite in equilibrium with tilleyite (CH49) would seem to correspond to a temperature in the range 710–720°C at 750 bars (Fig. 16), and to a somewhat lower temperature at lower pressure of H₂O, in agreement with that inferred above from the appearance of vesuvianite in the granular patches in UCV9 (T < 712°C); this temperature was thus considered to have been achieved after the end of the vein stage.

Pyroxene veins and endoskarms of the first stage

The conditions of stability during the development of the network of pyroxene veins in the marble at UCV (Fig. 18) have been calculated for one of the most Al-rich pyroxene compositions (Di₄₈, #4/45, similar to the relict endoskarn pyroxene in UCVZ #10/43), and for a typical pyroxene in contact with calcite (Di₇₀, #1/2).

At 750°C, the garnet – spinel – pyroxene association of the veins is in equilibrium with calcite (eq. 28) under a CO₂ pressure ranging from 95 bars (for the pyroxene in contact with calcite) to 240 bars (for the most Al-rich one). Melilite would appear instead of pyroxene at a lower pressure of CO₂, shown for the usual composition of melilite (Gh₆₀) and also for the compo-

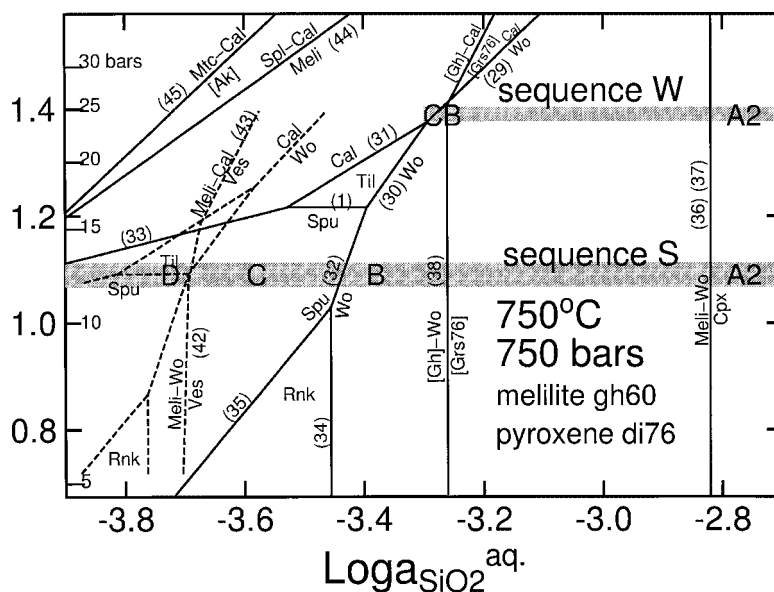


Fig. 17. Stability fields of the minerals from sequences S and W as function of pressure of CO_2 and activity of aqueous SiO_2 , calculated in the system $\text{SiO}_2\text{-CaO-Al}_2\text{O}_3\text{-MgO-H}_2\text{O-CO}_2$ at 750°C (solid lines) and 730°C (dashed lines). The approximate locations of the zones A to D are indicated for each sequence. Abbreviations and reaction stoichiometries are presented in Table 9.

sition (Gh_{64}) at equilibrium with the calcite – spinel – pyroxene (Di_{70}) association. According to the previously proposed interpretation of these veins as originating from apophyses of the monzodiorite, the observed association of minerals would correspond to their recrystallization (and leaching of Si, K, Na, Fe) under comparatively high pressures of CO_2 . The plagioclase compositions represented correspond to the range (An_{35} to An_{70}) observed in the monzodiorite. The reaction between calcitic marble, diopside and anorthite component of plagioclase, for example, is expected to produce garnet and aluminian pyroxene (eq. 26); the pyroxene would become enriched in Al until feldspar is exhausted (e.g., composition #4/45, Table 4). Further reaction of pyroxene with calcite would produce spinel and garnet and a more diopside-rich pyroxene (eq. 28; e.g., compositions #1/18, #1/2).

DISCUSSION AND CONCLUSIONS

The changes in CO_2 and SiO_2 contents of the fluid through metasomatic reactions

The pressure of CO_2 corresponding to the associations of skarn mineral depends on the initial composition of the fluid and on the exchange of CO_2 and SiO_2 between fluid and rock according to reactions such as, for example, the replacement of calcite by spurrite (eq.

33, Table 9). In a marble composed only of calcite, the amount of CO_2 produced by this reaction is limited by the availability of Si in the fluid. As the fluid in equilibrium with spurrite at 750°C , 750 bars has a maximum concentration of silica of $2.9 \times 10^{-4} m$, the maximum change in the CO_2 concentration in the fluid due to the replacement of calcite by spurrite, corresponding to the exhaustion of aqueous silica, is 8.7×10^{-4} mole/kg H_2O , or, when expressed as pressure, 10^{-2} bars. Even in the case of a quartz-saturated fluid ($0.046 m$), with a pressure of CO_2 high enough to allow for a direct replacement of calcite by wollastonite, the gain in pressure of CO_2 would be no more than 0.6 bars. The small influence of skarn-forming reactions on the pressure of CO_2 , in contrast with their major effect on the concentration of silica in the fluid, implies that the mineral association that developed under a small to moderate H_2O :rock ratio corresponds to the CO_2 pressure of the infiltrating fluid, whereas its SiO_2 activity is strongly influenced by the SiO_2 content of the original rock, i.e., CO_2 is perfectly mobile whereas SiO_2 is inert, according to the terminology of Korzhinskii (1970).

A more important source of CO_2 in exoskarn-forming processes may be the dissolution of calcite, which mostly depends on the HCl content of the fluid. The HCl content of the high-temperature, low-pressure fluid is expected to be high owing to the general tendency of ratios such as HCl/NaCl and HCl/KCl to increase with

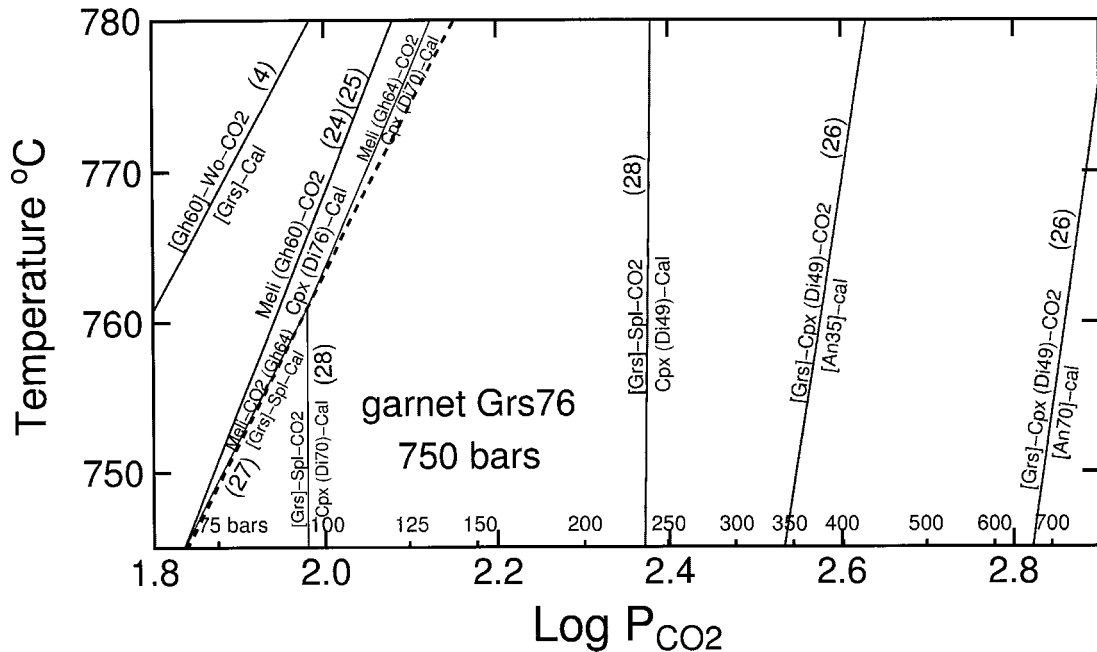


FIG. 18. Stability conditions of the aluminian-diopside-bearing associations of the first-stage endoskarms (veins in the marble and inclusions in endoskarn UCVZ), calculated in the system $\text{SiO}_2\text{-CaO-Al}_2\text{O}_3\text{-MgO-H}_2\text{O-CO}_2$.

increasing temperature and with decreasing pressure, where the fluid is buffered by a mineral association, such as is the case in those unmixing from a crystallizing magma (Shade 1974, Montoya & Hemley 1975, Popp & Frantz 1980, Sverjensky *et al.* 1991). This tendency, displayed by HCl-rich volcanic gases, has been investigated by Shinohara & Fujimoto (1994) at 600°C in the system albite – andalusite – quartz – H_2O – HCl. At 400 bars, the HCl molality of the vapor phase reaches 0.5 *m*, with a molality of NaCl of 0.3 *m*. Compared to the system $\text{H}_2\text{O-NaCl}$, the addition of HCl strongly increases the concentration of Cl that can be reached by the H_2O -rich fluid phase at low pressure without unmixing a brine (which would contain 75 wt.% NaCl in this case). With the assumption that the skarns of the vein stage formed in response to aqueous fluids of magmatic origin, these were probably in large part HCl-rich and able to dissolve calcite. An initial HCl content of 0.5 *m* would result in the dissolution of 0.25 moles CaCO_3 per kg H_2O , and an increase in pressure of CO_2 of 3.4 bars (Appendix).

Therefore, the changes in the pressure of CO_2 through fluid – marble interaction are expected to be small and mainly controlled by the initial HCl content of the fluid. As lower-pressure conditions result in a higher HCl content, the difference between the two sequences might be partly related to the difference in H_2O

pressure at the magmatic stage, found to be lower at UCV than at CH.

The expected major changes in the silica content of the fluid are consistent with the observed sequences of zones. In the well-defined range of CO_2 pressure of sequence W, the melilite – wollastonite association is stable under a narrow range of silica concentration, below which the association is melilite – calcite. Accordingly, wollastonite is replaced by calcite within vein BV, and calcite – wollastonite is the usual association of the exoskarn at UCV. In a similar way, the development of wollastonite instead of spurrite or tilleyite at the endoskarn – exoskarn boundary in many samples at CH can be accounted for by an only slightly higher concentration of silica, such as that resulting from a higher H_2O :rock ratio. In contrast, owing to the small dependence of the calcite – spurrite boundary on SiO_2 activity (Fig. 17), for a pressure of CO_2 in the range inferred at CH, spurrite (or tilleyite) is stable instead of calcite even under an extremely low concentration of silica. In accordance, the marble was widely replaced by spurrite and tilleyite in sequence S.

Origin of melilite, spurrite and tilleyite

The striking difference in pressure of CO_2 between the aluminian diopside veins and the melilite-bearing

associations implies that the CO₂-poor fluid responsible for the melilite stage circulated only in very small amounts in the region of the sample UCV4-1. Recrystallization of the pyroxene-bearing associations has been observed, with a large range of pyroxene compositions, which indicates a lack of equilibration, in accordance with the previously stated hypothesis and with the assumption that the pyroxene veins represent remnants of an early association developed at the margins of the intrusive rock (and along its apophyses) by a CO₂-rich fluid, as the first-stage endoskarns. Owing also to the tendency toward silica depletion of the fluid associated with this first stage, as proved by the crystallization of perovskite and of silica-deficient pyroxene, the surrounding marble may be assumed to have played the role of local source for this fluid, the origin of which remains unconstrained.

The spurrite – melilite – perovskite association in CH49 has already been interpreted as also indicative of a limited influence of the vein-stage fluid, although both the presence of melilite and the low pressure of CO₂ implied by spurrite are typical of this stage. One of its peculiarities is the higher undersaturation of this association in silica with respect to the melilite – wollastonite association in the veins and endoskarns. At the immediate contact of these veins, the exoskarn consists of wollastonite, which implies an input of Si on the marble side of the vein system. Even more silica-rich is the melilite-free zonation of CH22, in which the wollastonite exoskarn is in contact with zone A3, and where the titanian garnet and the evidence of Mg leaching are witnesses of the influence of the vein-forming fluid. As the silica undersaturation of the first stage is expected to persist to some extent through the vein stage, variations in silica activity of the associations developed by the vein fluid along the endoskarn – exoskarn boundary may result from an irregular development of either the primary skarns or the vein-stage skarns. Taking into account the comparatively high solubility of silica in high-temperature aqueous fluids, the persistence of a strong depletion in silica over a large part of the endoskarns indicates that the overall amount of fluid involved in the vein stage was not very large.

As a conclusion, we believe that melilite as well as spurrite and tilleyite are the result of the circulation of the vein-stage fluid at the boundary between the marble and the earlier-formed grossular – aluminian diopside endoskarns, strongly depleted in Si (and also Fe, Na and K) compared to the original monzodiorite. Many lines of evidence suggest that this fluid was exsolved from lower parts of the intrusive body at the pegmatite-forming stage: (1) its capacity to transport elements usually characterized by a low mobility, (2) its temperature range, similar to that found for the end of the two-feldspar crystallization in the monzodiorite, (3) the pegmatite-like texture observed at UCV, and (4) the deposition at the end of this stage of P-, S- and F- bearing minerals (ellestadite, cuspidine).

ACKNOWLEDGEMENTS

We are grateful to the Geological Institute of Romania for providing logistical support during the field work. Thanks are due to I. Katona for providing additional samples, organizing field work and taking photographs, to H. Remy and C. Richard for technical assistance in performing the numerous electron-microprobe analyses, to S. Baudesson, G. Badin and G. Drouet for preparing the thin sections, to M.N. Sarcia for drawing the figures, and to P. Sonnet for helpful discussions. We are especially indebted to Danielle Velde, whose interest and advice throughout this study have been greatly appreciated. We also thank B. Moine and an anonymous reviewer for interesting and fruitful comments on a first version of this paper.

REFERENCES

- BERMAN, R.G. (1988): Internally-consistent thermodynamic data for minerals in the system Na₂O–K₂O–CaO–MgO–FeO–Fe₂O₃–Al₂O₃–SiO₂–TiO₂–H₂O–CO₂. *J. Petrol.* **29**, 445-522.
- BURNHAM, C.W. (1959): Contact metamorphism of magnesian limestones at Crestmore, California. *Geol. Soc. Am., Bull.* **57**, 879-928.
- _____ (1979): Magmas and hydrothermal fluids. In *Geochemistry of Hydrothermal Ore Deposits* (2nd edition, H.L. Barnes, ed.). John Wiley and Sons, New York, N.Y. (71-136).
- CHARLU, T.V., NEWTON, R.C. & KLEPPA, O.J. (1981): Thermochemistry of synthetic Ca₂Al₂SiO₇ (gehlenite) – Ca₂MgSi₂O₇ (åkermanite) melilites. *Geochim. Cosmochim. Acta* **45**, 1609-1617.
- DEER, W.A., HOWIE, R.A. & ZUSSMAN, J. (1986): *Rock-Forming Minerals*. **5. Non-Silicates** (2nd edition). Longman, London, U.K.
- GREEN, N.L. & USDANSKY, S.I. (1986): Ternary-feldspar mixing relations and thermobarometry. *Am. Mineral.* **71**, 1100-1108.
- GROSS, S. (1977): The mineralogy of the Hatrum Formation, Israel. *Bull. Geol. Survey Israel* **70**.
- GUNTER, W.D. & EUGSTER, H.P. (1978): Wollastonite solubility and free energy of supercritical aqueous CaCl₂. *Contrib. Mineral. Petrol.* **66**, 271-281.
- GUY, B., SHEPPARD, S.M.F., FOUILLAC, A.M., LE GUYADER, R., TOULHOAT, P. & FONTEILLES, M. (1988): Geochemical and isotope (H,C,O,S) studies of barren and tungsten-bearing skarns of the French Pyrenees. In *Mineral Deposits within the European Community* (J. Boissonas & P. Omenetto, eds.). Springer, Berlin, Germany (53-75).
- HARKER, R.I. & TUTTLE, O.F. (1956): The lower limit of stability of åkermanite (Ca₂MgSi₂O₇). *Am. J. Sci.* **254**, 468-478.

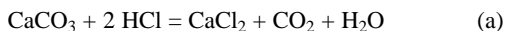
- HENMI, C., KUSACHI, I., HENMI, K., SABINE, P.A. & YOUNG, B.R. (1973): A new mineral bicchulite, the natural analogue of gehlenite hydrate, from Fuka, Okayama Prefecture, Japan and Carneal, County Antrim, Northern Ireland. *Mineral. J.* **7**, 243-251.
- HENMI, K., KUSACHI, I. & NUMANO, T. (1971): Contact minerals from Kushiro, Hiroshima Prefecture. I. Gehlenite and hydrogrossular. *J. Mineral. Soc. Japan* **10**, 160-169.
- HOLLAND, T.J.B. & POWELL, R. (1998): An enlarged and updated internally consistent thermodynamic dataset with uncertainties and correlations: the system K_2O - Na_2O - CaO - MgO - MnO - FeO - Fe_2O_3 - Al_2O_3 - TiO_2 - SiO_2 - C - H_2O - O_2 . *J. Metamorph. Geol.* **8**, 89-124.
- HUGHES, C.J. (1960): An occurrence of tilleyite-bearing limestones in the Isle of Rhum, Inner Hebrides. *Geol. Mag.* **97**, 384-388.
- ISTRATE, G., ȘTEFAN, A. & MEDEȘAN, A. (1978): Spurrite and tilleyite in the Cornet Hill, Apuseni Mountains, Romania. *Rev. Roumaine Géol., Géophys. et Géogr., Géologie* **22**, 143-153.
- JAMTVEIT, B., BUCHER-NÜRMINEN, K. & STIJFHOORN, D.E. (1992): Contact metamorphism of layered shale-carbonate sequences in the Oslo Rift. I. Buffering, infiltration and the mechanisms of mass transport. *J. Petrol.* **33**, 377-422.
- _____, DAHLGREN, S. & AUSTRHEIM, H. (1997): High-grade contact metamorphism of calcareous rocks from the Oslo Rift, southern Norway. *Am. Mineral.* **82**, 1241-1254.
- JOESTEN, R. (1974): Pseudomorphic replacement of melilite by idocrase in a zoned calc-silicate skarn, Christmas Mountains, Big Bend region, Texas. *Am. Mineral.* **59**, 694-699.
- _____ & FISHER, G. (1988): Kinetics of diffusion-controlled mineral growth in the Christmas Mountains (Texas) contact aureole. *Geol. Soc. Am., Bull.* **100**, 714-732.
- KORZHINSKII, D.H. (1970): *Theory of Metasomatic Zoning*. Clarendon, Oxford, U.K.
- MANNING, C.E. (1993): The solubility of quartz in H_2O in the lower crust and upper mantle. *Geochim. Cosmochim. Acta* **58**, 4831-4839.
- MARINCEA, Ș., BILAL, E., VERKAEREN, J., PASCAL, M.-L. & FONTEILLES, M. (2001): Superposed parageneses in the spurrite-, tilleyite- and gehlenite-bearing skarns from Cornet Hill, Apuseni Mountains, Romania. *Can. Mineral.* **39**, 1435-1453.
- MONTOYA, J.W. & HEMLEY, J.J. (1975): Activity relations and stabilities in alkali feldspar and mica alteration reactions. *Econ. Geol.* **70**, 577-583.
- NOCKOLDS, S.R. (1947): On tilleyite and its associated minerals from Carlingford, Ireland. *Mineral. Mag.* **28**, 151-158.
- PERCHUK, L.L. & ARANOVICH, L.Y. (1979): Thermodynamics of minerals of variable composition: andradite-grossularite and pistacite-clinozoisite solid solutions. *Phys. Chem. Minerals* **5**, 1-14.
- PIRET, R. (1997): *Minéralogie et géochimie des skarns de haute température des régions de Magureaua Vatei et de Cornet Hill (Monts Apuseni)*. Mémoire de Licence, Université Catholique de Louvain, Belgique.
- POPP, R.K. & FRANTZ, J.D. (1980): Mineral-solution equilibria. III. The system Na_2O - Al_2O_3 - SiO_2 - H_2O - HCl . *Geochim. Cosmochim. Acta* **44**, 1029-1037.
- REVERDATTO, V.V. (1970): Pyrometamorphism of limestones and the temperature of basaltic magmas. *Lithos* **3**, 135-143.
- _____, PERTSEV, N.N. & KOROLYUK, V.N. (1979): PCO_2 -T-evolution of zoning in melilite during the regressive stage of contact metamorphism in carbonate-bearing rocks. *Contrib. Mineral. Petrol.* **70**, 203-208.
- SABINE, P.A. (1975): Metamorphism processes at high temperature and low pressure: the petrogenesis of the metasomatized and assimilated rocks of Carneal, Co. Antrim. *Phil. Trans. R. Soc.* **A280**, 225-269.
- SACK, R.O. & GHIORSO, M.S. (1994a): Thermodynamics of multicomponent pyroxenes. I. Formulation of a general model. *Contrib. Mineral. Petrol.* **116**, 277-286.
- _____ & _____. (1994b): Thermodynamics of multicomponent pyroxenes. III. Calibration of $Fe^{2+}(Mg)_{-1}$, $TiAl_2(MgSi_2)_{-1}$, $TiFe^{3+}_2(MgSi_2)_{-1}$, $AlFe^{3+}(MgSi)_{-1}$, $NaAl(CaMg)_{-1}$, $Al_2(MgSi)_{-1}$ and $Ca(Mg)_{-1}$ exchange reactions between pyroxenes and silicate melts. *Contrib. Mineral. Petrol.* **118**, 271-296.
- SHADE, J.W. (1974): Hydrolysis reactions in the SiO_2 -excess portion of the system K_2O - Al_2O_3 - SiO_2 - H_2O in chloride fluids at magmatic conditions. *Econ. Geol.* **69**, 218-228.
- SHINOHARA, H. & FUJIMOTO, K. (1994): Experimental study in the system albite - andalusite - quartz - $NaCl$ - HCl - H_2O at 600°C and 400 to 2000 bars. *Geochim. Cosmochim. Acta* **58**, 4857-4866.
- ȘTEFAN, A., ISTRATE, G. & MEDEȘAN, A. (1978): Gehlenite in calc-skarns from the Magureaua Vatei-Cerboia (Apuseni Mountains - Romania). *Rev. Roumaine Géol., Géophys. et Géogr., Géologie* **22**, 155-160.
- SVERJENSKY, D.A., HEMLEY, J.J. & D'ANGELO, W.M. (1991): Thermodynamic assessment of hydrothermal alkali feldspar - mica - aluminosilicate equilibria. *Geochim. Cosmochim. Acta* **55**, 989-1004.
- TILLEY, C.E. (1929): On larnite (calcium orthosilicate, a new mineral) and its associated minerals from the limestone contact-zone of Scawt Hill, Co. Antrim. *Mineral. Mag.* **22**, 77-86.
- _____. (1948): The gabbro - limestone contact zone of Camas Mor, Muck, Invernessshire. *Bull. Comm. Géol. Finlande* **140**, 97-104.

- _____ (1951): A note on the progressive metamorphism of siliceous limestones and dolomites. *Geol. Mag.* **88**, 175-178.
- UCHIDA, E. & IYAMA, J.T. (1981): On kamaishilite, $\text{Ca}_2\text{Al}_2\text{SiO}_6(\text{OH})_2$, a new mineral dimorphous with bicchulite from the Kamaishi mine, Japan. *Proc. Japan. Acad.* **57**, ser. **B**, 239-243.
- WIECHMANN, M.J. (1995): *Contact Metamorphism and Skarn Formation at Crestmore, California*. Ph.D. thesis, Johns Hopkins Univ., Baltimore, Maryland.
- WILLEMSE, J. & BENSCH, J.J. (1964): Inclusions of original carbonate rocks in gabbro and norite of the eastern part of the Bushveld complex. *Trans. Geol. Soc. S. Afr.* **67**, 1-87.

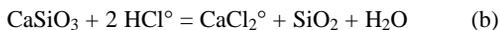
Received January 6, 2000, revised manuscript accepted August 31, 2001.

APPENDIX : CALCITE SOLUBILITY IN A CHLORIDE-BEARING FLUID

Calcite is dissolved in a chloride fluid according to reaction (a):



CaCl_2 is not appreciably dissociated at the temperature and pressure conditions of formation estimated for the skarn. However, owing to the possible contribution of $\text{Ca}(\text{OH})_2$, consideration of this reaction only provides a minimum estimation of the solubility of calcite. Owing to the low density of the fluid, the equations of state for aqueous species do not allow us to calculate the equilibrium constant, but an order of magnitude can be obtained from the experimental study of the equilibrium between wollastonite, quartz and chloride fluid (Gunter & Eugster 1978):



The corresponding equilibrium constant, K_b , is expressed by $\log K_b = \log a(\text{CaCl}_2^\circ) - 2 \log a(\text{HCl}^\circ) + \log$

$a(\text{H}_2\text{O})$, and measured as $\log K_b \approx \log m(\text{CaCl}_2) - 2 \log m(\text{HCl}) + \log a(\text{H}_2\text{O}) = 1.78$ (1 kilobar) and 2.49 (2 kilobars), assuming that CaCl_2° was the main aqueous species of Ca and conventionally taking the activity coefficients of uncharged aqueous species as 1.

Under the same assumptions, the constant of equilibrium (a) is calculated from K_b and the thermodynamic data for wollastonite, quartz, calcite and CO_2 from the THERMOCALC database: $\log K_a = \log a(\text{CaCl}_2^\circ) - 2 \log a(\text{HCl}^\circ) + \log a(\text{H}_2\text{O}) + \log f(\text{CO}_2) \approx 5.40$ (1 kilobar) and 6.22 (2 kilobars).

If the reaction ΔV remained constant between 0.75 kilobar and 2 kilobars, $\log K_a$ would be 5.2 at 0.75 kbar, and the ratio $a(\text{CaCl}_2^\circ)/a(\text{HCl}^\circ)^2$ at equilibrium with calcite would be about $10^{3.8-4.0}$ for CO_2 pressure in the range 15 – 30 bars. Although the assumption of constant ΔV is probably a poor one, the ratio $m(\text{CaCl}_2)/m(\text{HCl})^2$ is large enough to ensure that the initial HCl content of the fluid would be quantitatively converted to CaCl_2 upon reaction with calcite.